Single-molecule chemistry

W. Ho

Citation: J. Chem. Phys. **117**, 11033 (2002); doi: 10.1063/1.1521153
View online: http://dx.doi.org/10.1063/1.1521153
View Table of Contents: http://jcp.aip.org/resource/1/JCPSA6/v117/i24
Published by the American Institute of Physics.

Single-molecule chemistry

W. Ho[a)]
Department of Physics and Astronomy and Department of Chemistry, University of California, Irvine, California 92697-4575

(Received 15 July 2002; accepted 18 September 2002)

The ability to probe individual atoms and molecules have made it possible to reveal properties which otherwise would be hidden in the study of an ensemble of atoms and molecules. The scanning tunneling microscope (STM) with its unmatched spatial resolution and versatility literally allows us to touch atoms and molecules one at a time and to carry out experiments which previously were only imagined. One of the great attributes of the STM is that it provides a real space view of the individual molecules and the atomic landscape of their environment, thus removing many of the uncertainties surrounding the nature of the system under study. Combining its imaging, manipulation, spectroscopic characterization, and chemical modification capabilities, the STM has enabled direct visualization of chemistry by revealing the fundamental properties of atoms and molecules and their interactions with each other and the environment. While femtosecond lasers have made it possible to study chemistry at the temporal limit, the STM provides an understanding of chemistry at the spatial limit. © *2002 American Institute of Physics.* [DOI: 10.1063/1.1521153]

I. INTRODUCTION

Nanoscience and nanotechnology are concerned with materials with dimensions that approach nanometers and below. Over the last few years this area of research has attracted a great deal of attention. The main reasons for this attraction lie in the prospect of understanding matter and its transformations at the most rudimental level and the hope that novel devices can be developed. The scientific activities are spurred by the invention of new tools, namely, the scanning probe microscopes and laser based techniques, the refinement of electron beam lithography, the synthesis of new materials, and the development of molecular self-assembly. Ultimately, the building blocks of all materials and devices are the individual atoms and molecules. The coming decades will be an exciting period of research and development with materials at the atomic and molecular level.

Why is it desirable and important to study single atoms and molecules? First, they are the basic building blocks of matter. Second, there are intrinsic properties of molecules that simply cannot be probed in an ensemble of molecules where average properties are measured. Third, the environment and its effects on individual molecules can be determined. Single atoms and molecules are sensitive to the energetic inhomogeneity and local potentials, e.g., adsorption at defect sites and spectral broadening. Fourth, the ability to observe single molecules makes it possible to manipulate and control chemistry at the spatial limit. Small systems exhibit properties which are hidden in larger systems and quantum mechanics becomes the governing rules. The study of single atoms and molecules provides new insights into quantum mechanics and the nature of chemical bonding that forms the critical bases for controlling the properties and functions of nanomaterials.

Lasers and scanning probes are arguably two of the most versatile and important tools which are being used widely by researchers in different disciplines. The ability of the scanning tunneling microscope (STM) to reveal images of individual atoms and molecules is simply astounding, as illustrated in Fig. 1. Since ''seeing is believing,'' results from the STM are visually convincing and often esthetically pleasing. One of the great attributes of the STM is that it provides a real space view of the atomic landscape of the solid surface, thus removing much of the uncertainties surrounding the nature of the system under study. The reason that the STM is such a versatile and powerful tool is that its operation involves tunneling electrons. It is the coupling of tunneling electrons to the electronic states and the nuclear motions that allows us to image, manipulate, spectroscopically characterize, and to dissociate and form bonds. As a scanning probe, the STM provides spatially resolved mapping of the topography and excitations of the materials surface with subangstrom resolution.

The STM literally allows us to touch atoms and molecules one at a time. The STM is ideally suited for the investigation of nanoscale chemical and physical phenomena with an emphasis on probing the basic properties of single atoms and molecules in their nanoenvironment on solid surfaces. The goal is to obtain detailed description of single atoms and molecules which form the basis for understanding chemical and physical processes on surfaces and properties of nanostructured condensed matter and molecular materials. These studies have technological implications such as in semiconductor processing, chemical catalysis, environmental remedy, magnetic storage, and in futuristic devices such as molecular electronics, spintronics, and quantum computers.

One of the drawbacks of the STM had been its lack of chemical sensitivity. The reason is that STM images are determined by the convolution of the electronic structure of the tip and the surface, which are difficult to interpret. We have demonstrated that chemical analysis with the STM is possible with inelastic electron tunneling spectroscopy (IETS)

a)Electronic mail: wilsonho@uci.edu

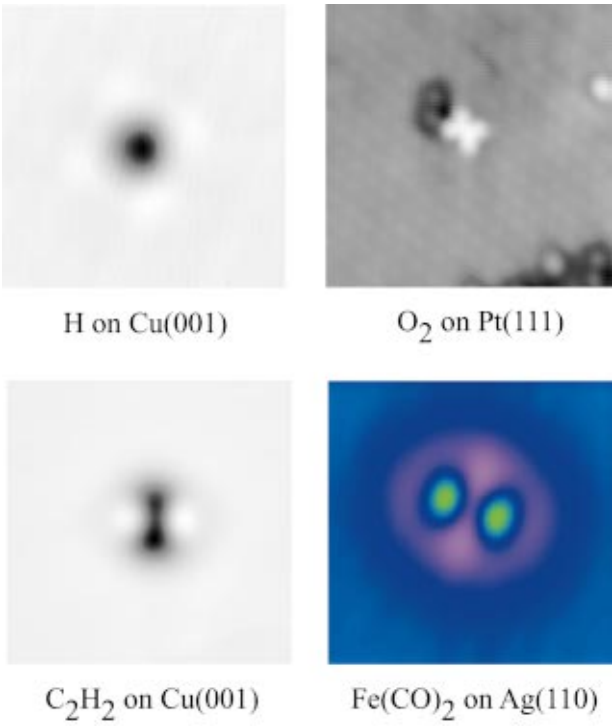

FIG. 1. (Color) STM topographic images of four single molecules on different metal surfaces, selected for the details they reveal. H on Cu(001) at 9 K: 15 Å×15 Å, the only image to date of a single hydrogen atom on a metal surface. O_2 on Pt(111) at 8 K: 36 Å×36 Å, exhibiting the π^* orbital. C_2H_2 on Cu(001) at 8 K: 25 Å×25 Å, showing the two hydrogen atoms as protrusions and the C–C bond as the central depression. $Fe(CO)_2$ on Ag(110) at 13 K: 25 Å×25 Å, synthesized by manipulated attachment of two CO molecules, the two protrusions, one at a time to a single Fe atom.

and have reached the limit of sensitivity of vibrational spectroscopy, that of a single bond. Vibrational spectroscopy has long served as a fingerprinting technique for chemical analysis of bulk samples. The ability to measure spatially resolved vibrational intensity with sub-angstrom resolution in single molecules makes it possible to directly determine quantitatively a number of fundamentally important physical and chemical processes.

Our homemade, variable temperature (8–350 K) STM operating in ultrahigh vacuum conditions ($<2\times10^{-11}$ Torr) is simple, versatile, and stable, enabling a wide range of problems to be successfully investigated. These include intramolecular energy transfer, the making of molecules one at a time, breaking of individual chemical bonds, controlling the pathways of chemical reactions, the observation of negative differential resistance, quantum tunneling of hydrogen atoms, the induction and visualization of conformational changes, rotational, and translational motions—all involving single atoms or molecules. STM provides us with new capabilities which allow unexpected observation of the intrinsic properties of molecules and the nature of their interactions with each other and the surroundings.

II. SINGLE-MOLECULE EXPERIMENTS

There are four main approaches to the study of single molecules.

A. Single-molecule optical spectroscopy

The first approach is based on the phenomenon of laser induced fluorescence (LIF). A dramatic demonstration of this approach is the direct observation of the discrete rotational motion of the γ-subunit of F1-ATPase, which is one part of the enzyme responsible for ATP synthesis and hydrolysis that are important steps in the energy cycles in the human body.[1] The experiment involves tagging an actin filament with molecules which fluorescence when irradiated with light. The discrete rotation is thus optically detected. Prior to this experiment, this rotational motion was postulated from studies of an ensemble of enzymes. It is only by studying a single molecule that such a rotational motion can be directly observed, thus putting to rest all doubts about the mechanism.

Although single-molecule optical spectroscopy was historically carried out first in the absorption mode,[2] the advantages of fluorescence[3] mode quickly became apparent. The fluorescence is redshifted from the excitation light which can be effectively filtered. To reduce further the background, the probe volume is kept small by tightly focusing the laser beam. Different geometries have been demonstrated in single-molecule optical spectroscopy, including near-field scanning optical microscopy (NSOM),[4] far field excitation,[5] electric field enhancement by irradiating a metallic tip,[6] and excitation with evanescent waves in a total internal reflection arrangement.[7]

Single-molecule optical spectroscopy was initially confined to a handful of polyaromatic molecules in crystalline or amorphous organic solids at liquid-He temperature because only these systems yielded sufficiently strong and narrow absorption and emission lines.[8] It was found that the emission lines of individual molecules shifted with time due to guest–host coupling, an effect that became known as spectral diffusion.[9] Time-resolved measurements were performed by time-correlated single-photon counting with time-resolution typically about 100 ps. Intersystem crossing into the first triplet state led to ''dark'' periods on the time scale of the triplet lifetime, giving rise to photon bunching.[3,10] During the ''light'' periods, the emitted photons are separated in time and exhibit antibunching.[11] Electron spin resonance was optically detected from single molecules in the triplet (''dark'') state.[12,13]

Advances in background suppression and detection efficiency opened the door to measurements of a wider range of fluorescent molecules, e.g., dyes, at room temperature.[4,14–18] Since then, molecular biology has arguably become the main benefactor of single-molecule optical spectroscopy.[19] Fluorescence resonance energy transfer (FRET) between a single pair of dye molecules was observed.[20] The efficiency of intramolecular electronic energy transfer was revealed from the spectroscopy of a conjugated polymer molecule with multiple chromophores.[21] It was found that the fluorescence from a protein in a jellyfish could be switched back on after photobleaching, which suggests a biological photonic switch with some potential applications.[22] The enzymatic turnover of a single fluorescent enzyme molecule was observed in real-time.[23] In addition to fluorescent dyes, semiconductor

quantum dots with tunable emissions can be used effectively as biological markers.[24,25]

There are two limitations to single-molecule fluorescence spectroscopy. First, not every molecule is fluorescent. Second, the fluorescent molecules tend to be affected by continuous illumination and become photobleached. However, single-molecule optical spectroscopy takes advantage of the attributes of optical spectroscopy, and can be applied to study molecules in solution, which makes it interesting for many chemical and biological problems. Although the spatial resolution is not sufficient for imaging on the molecular level, single-molecule optical spectroscopy does allow the tracking of molecular motion on the nanometer scale.

B. Optical tweezers

The second approach for studying single molecules involves the use of the optical tweezer or the laser trap, which allows manipulation and measurement of forces acting on single molecules.[26,27] In an electric field gradient, an approximately 1 μm diam dielectric sphere (e.g., silica, polystyrene, latex) attached to the macromolecule is drawn toward and is trapped at the focus of a laser beam. Transparent beads are attached to one or both ends of the molecule and are controlled by one or a pair of optical tweezers. Flow cells are often used to stretch the chainlike molecules. The trapping is observed with an integrated optical microscope. In the near-focus region, the attractive force acting on the bead is proportional to the distance from the focus, thus allowing the force acting on the molecule to be measured by detecting the position of the bead. Forces in the picoNewton range can be correlated with nanometer motions.

Optical tweezers have enabled the study of biological molecular motors. For example, it has been used successfully to quantitatively measure the motions of linear motors in biological systems such as the translation of the RNA polymerase along the DNA in the transcription of the DNA to the RNA.[28] The force that is exerted by the RNA polymerase on the DNA is measured from the displacement of the dielectric sphere attached to the DNA. Similarly, single-molecule mechanics have also elucidated the motions of motor proteins myosin,[29,30] kinesin,[31–33] dynein,[34] and the reversible unfolding of the protein titin.[35,36] Magnetic beads, instead of optical tweezers, have also been used successfully to investigate the elasticity of single DNA molecules.[37,38] While unattached molecules are too small to be trapped,[27] optical tweezer can manipulate whole cells or organelles in living cells without damaging them.[39]

C. Molecular conductance: *I–V* spectroscopy

Advances in electron beam lithography, control over electrode geometry, and the synthesis of appropriate molecules have made it possible to measure the conductance of single molecules fixed between the two electrodes. Thiols are commonly used and the sulfur atoms anchor the molecules to the gold electrodes. Different methods have been used to measure the molecular conductivity: locating a thiol molecule in the junction of a scanning tunneling microscope,[40] bridging the gap of a break junction formed by a piezo-driven wedge with a single thiol molecule,[41] and the diffusion of a single molecule to the gap of an electromigration-induced break junction.[42,43] Since it has not been possible to image single molecules in the break junctions, it remains uncertain as to how the molecule is bonded to the electrodes.

If nanotubes are considered as single molecules, they constitute the most widely studied molecules whose electrical conductivity have been measured in a variety of configurations. The long length of nanotubes allows contacts to be made using nanostructured metal electrodes fabricated by electron beam lithography. Because of their unique properties, including the dependence of metallic and insulating behavior on the wrapping angle,[44,45] a variety of conductivity measurements have been made with a continuing increase in the fabrication sophistication.[46–53]

D. Scanning probe microscopy

The fourth approach for studying single molecules is based on the scanning probes: the atomic force microscope and the scanning tunneling microscope.

1. Atomic force microscope

While the atomic force microscope (AFM) (Refs. 54–56) is capable of atomic and molecular spatial resolution, it is usually difficult to achieve. In the AFM, the forces acting on a tip mounted on a small cantilever beam are detected by monitoring the cantilever deflection. The acknowledged strengths of the AFM are tied to the fact that the operation of the AFM does not require a current through the sample. The AFM can be operated on any substrate, insulating as well as conducting, in aqueous solutions, and can image large ''three-dimensional,'' nonconducting molecules. Thus the AFM can be used to study organic molecules in various surroundings as well as biological molecules under conditions resembling their natural occurrence.[57–59]

In chemical force microscopy (CFM), the imaging power of the AFM is increased by making the tip sensitive to particular chemical functional groups.[60–62] CFM has been performed by attaching monolayers of specific molecules to an AFM tip. However, spatial resolution better than several nm has not yet been achieved. This might change with the use of single-wall carbon nanotubes to chemically modify the tip.[63,64] In magnetic resonance force microscopy (MRFM), the sample is immersed in a magnetic field gradient, a dc applied magnetic field, and a radio frequency radiation.[65] Although MRFM makes the AFM a spectroscopic tool, its sensitivity is still far from the single-molecule level.

The AFM has been used effectively to manipulate single large organic molecules (e.g., polymers) and biomolecules (e.g., proteins) while simultaneously measuring their elastic restoring force. Two kinds of measurements that are fundamentally important in molecular biology can now be performed on individual molecules. First, the reversible folding–unfolding of protein chains yields characteristic stick-slip patterns that provide insight into the folding patterns of the proteins.[66,67] The experiments involve stretching a single protein molecule that has been chemically attached between the AFM tip and the substrate. Similar experiments

can be performed on individual polymer molecules.[68] Second, the forces between two complementary biomolecules, e.g., ligand–receptor[69,70] or antibody–antigen[71,72] pairs, can be measured by attaching one molecule to the substrate and its counterpart to the tip. The forces are in the picoNewton–nanoNewton range, well accessible by the AFM.

2. Scanning tunneling microscope

The scanning tunneling microscope (STM) can probe single molecules with atomic resolution and reveal their quantum properties. Since the STM relies on a tunneling current between the tip and the sample, a conductive substrate is required, e.g., metals, semiconductors, and ultrathin oxide on metals or semiconductors. Typical bias voltage and current are ~ 0.1 V and ~ 1 nA, and the tunneling gap is ~ 6 Å. The current, energy of the electrons (as given by the bias voltage), and electric field could influence the molecule in the junction such that the measurements are in error. Since all scientific measurements require some interactions of the probe with the system, it is necessary to understand and control the magnitude of such interactions. By reducing the voltage and current between the tip and the sample, perturbations of the single molecules in the junction are minimized and any effects can be made insignificant compared to the chosen response of the system being measured.

Tunneling electrons from an STM can be used to excite and induce changes in a molecule. From these changes, detailed properties of the molecules are revealed. The phenomenon of tunneling is one of the wonders of quantum mechanics, and the STM has allowed us to probe and visualize materials from the bottom up, starting with single atoms and molecules. However, the topographic images, recorded at constant current or density of states, are difficult to interpret especially as the number of atoms in the molecule increases.[73] Results from tunneling spectroscopy probing the filled or empty electronic states of the molecule are often not straightforward to interpret. The excited states of adsorbed molecules are shifted and broadened due to interactions with the substrate, e.g., C_{60} (Refs. 74, 75) and Cu(II)etioporphyrin-I,[76] and are difficult to treat by theoretical calculations. Since electronic states are often located a few electronvolts away from the Fermi level, the high energy of the tunneling electrons and the high electric field are more likely to perturb the molecule, leading to translation and dissociation. Such effects can be determined but limit the application of electronic spectroscopy with the STM. However, it is desirable to carry out electronic spectroscopy since knowledge of the electronic states is important for chemical identification and in understanding the electronic structure, electrical conductivity, light emission, chemical reactivity, and magnetic properties of single molecules.

Inelastic electron tunneling spectroscopy with the STM (STM-IETS) probes the vibrational properties of single molecules.[77] The energies and intensities of the spectral features are characteristic of the chemical bonds and their interactions with the surrounding medium. Chemical sensitivity can thus be obtained. In addition, the molecules are not perturbed in STM-IETS since low energy tunneling electrons are involved. One of the great attributes of vibrational spectroscopy lies in the amount of information that can be obtained without theoretical analysis. In addition to achieving the limit of sensitivity of vibrational spectroscopy, that of a single bond, vibrational microscopy can be used to image the spatial distribution of the vibrational intensity.

Tunneling electrons from the STM can also induce light emission from surfaces with adsorbed molecules such as C_{60}.[78,79] Recent experiments have shown, however, that the observed light emission comes from plasmon emission from the substrate, modified by the molecule, and not directly from the adsorbed molecule.[80] By isolating the molecule from the substrate with an ultrathin oxide layer, direct emission of light from the molecule may be observed.[81] The coupling of photon spectroscopy with the spatial resolution of STM is expected to provide new information on single molecules adsorbed on surfaces. In addition, new insights into electron dynamics and energy flow in single molecules on surfaces can be obtained from understanding the mechanism of photon emission.

III. SINGLE-MOLECULE VIBRATION

A. Different methods

Single-molecule vibrational spectroscopy has been achieved with the STM (Ref. 77) and optical techniques using lasers.[82–86] Vibrational spectroscopy provides the most direct chemically sensitive analysis of single molecules adsorbed on surfaces.

Single-molecule vibrationally resolved fluorescence was obtained from a dilute concentration of pentacene in *p*-terphenyl crystal at liquid helium temperature.[82,87] The appearance of vibronic structures in the fluorescence spectra have been observed to date for polycyclic aromatic molecules in organic host matrices at cryogenic temperatures. While the spectral features, such as energy and intensity of the peaks, reflect, in principle, the nature of the interactions between the molecules and the host, a precise explanation is difficult. Thus vibronic single-molecule spectroscopy in solids has not been extended beyond feasibility demonstration. Higher vibrational effects involving hyper-Raman and subharmonic resonances have also been observed.[88] Due to resonant electronic excitation, photobleaching of single molecules is a problem in single-molecule optical spectroscopy. The molecules are believed to have changed conformation or chemically transformed, leading to optical inactivity.

Raman spectroscopy claiming single-molecule sensitivity has been reported for crystal violet dye molecule dissolved in aqueous colloidal silver solution[83] and rhodamine 6G adsorbed on colloidal silver particles immobilized on polylysine-coated glass substrate.[84] The feasibility of the experiments relies on the observation that Raman scattering is strongly enhanced for molecules which are adsorbed at particular sites on the surface of Ag or Au particles with nominal diameters of ~ 10 nm to 1 μm. The enhancement factor is extremely high, up to 10^{14}, allowing nonresonant Raman spectroscopy, which reduces the probability of photobleaching and makes it possible to detect nonfluorescent molecules.[83,89] Anti-Stokes Raman scattering has also been observed on single dye molecules.[90] Single-molecule surface

enhanced Raman scattering has been reported mostly for dye molecules,[83,84,90–95] but also have been extended to hemoglobin[96] and DNA fragments.[89] The identification of single nucleotides in DNA sequencing is one promising future applications of surface enhanced Raman scattering.[89,97]

The origin of this extremely large enhancement continues to be under debate.[98,99] Increase in the electric field, chemical effects, and excitation of plasmon resonances in the metal particles certainly contribute to the overall enhancement. In some cases, the aggregation of metal particles to form larger structures[89] or the addition of electrolytes[100] have been reported to increase the effect. Critical to the understanding is the observation that only a small fraction of the metal particles are ''hot,'' i.e., show Raman enhancement in the 10^{14} range.[84] This observation led to the hope that by suitable preparation of the particles, the enhancement factor can even be increased and the majority of the particles can be ''hot.'' [91]

Enhancement of Raman scattering cross section has also been reported using an AFM tip instead of the metallic particles.[85,86] By combining an AFM with a scanning near-field optical microscope, Raman spectra were obtained from a thin cresyl blue dye layer deposited on glass with a silver coated tip and from C_{60} film with a gold tip.[85] Most significant is the observation that the intensity of the Raman peaks decreased substantially when the tip was retracted.[85] By combining an AFM with a Raman microprobe and coating the tip with gold, a Raman spectrum was obtained after transferring $\sim$10 femtograms of C_{60} to the tip.[86] In addition, surface enhanced Raman effect was observed from a sulfur film.[86] The Raman signal became undetectable when the laser light was focused on the surface instead of the tip.[86] Although these experiments were carried out on thin films, single-molecule detection should in principle be achievable.

Infrared absorption spectroscopy on single molecules has not been reported. This is a difficult task due to the lack of sufficiently sensitive infrared detector. In addition, absorption measurement requires detecting small changes in a large signal. It is also difficult to imagine the use of coherent anti-Stokes Raman scattering (CARS) (Ref. 101) for single-molecule spectroscopy. In CARS, molecules are vibrationally excited by the difference frequency between two pump laser beams, and the vibrational excitation is probed by a third photon beam, and the anti-Stokes Raman signal is detected. CARS is thus a four-wave mixing technique. Three-dimensional imaging with $\sim$300 nm resolution has been demonstrated.[101]

One general limitation of single-molecule optical spectroscopy lies in the spatial resolution. It is possible to overcome the diffraction limit by using near-field scanning optical microscopy, yielding a spatial resolution of tens of nanometers.[4,5] Light is guided to the sample via a metal-coated optical fiber. The heat generated in the fiber, however, limits the intensity of the incident light. Moderate intensities are required for surface enhanced Raman spectroscopy, accounting for the use of far-field illumination in measurements performed to date.

Inelastic electron tunneling spectroscopy with the STM (STM-IETS) provides the highest spatial resolution for vibrational spectroscopy and microscopy. In fact, the unmatched spatial resolution extends to tunneling spectroscopy in general. The spatial resolution of spectroscopy and microscopy with the STM is as good as that for topographic images. The combination of vibrational spectroscopy and microscopy with sub-angstrom resolution has provided unique insights into the properties and chemistry of single molecules.

B. STM-IETS: Vibrational spectroscopy and microscopy

The basic principles of operation of the STM are quite simple. A metallic tip is brought very close to the surface, $\sim 5-10$ Å, and a voltage is applied between the sample and the tip. At these distances, a current flow due to tunneling is detected. The operation of the STM can be replaced by an equivalent circuit consisting of a power supply and a resistor. For a metallic tip and sample, the junction resistance is typically 1 MΩ to 1 GΩ. The resistor, however, is of atomic dimensions. When the atom or molecule in the junction moves, such as in translation, rotation, vibration, conformational change, or bond dissociation and formation, the resistance changes. By holding the tunneling distance fixed, changes in resistance are reflected in the corresponding changes in the current. When the power supply output, i.e., the sample bias, is held fixed, the current is monitored as a function of time. By varying the sample bias, spectroscopic information is obtained from the $I-V$ curves. From these changes in the current, properties of the single atom or molecule in the junction can be derived. These operational conditions for the STM are illustrated in Fig. 2.

Optical techniques have dominated spectroscopic investigation of materials ranging from atoms and molecules to solids. With the invention of the STM, noninvasive, spatially resolved spectroscopy has become possible. All the spectroscopic information are contained in the $I-V$ curves, the analog of recording the system's response as a function of the wavelength in optical spectroscopy. Tunneling is predominantly an elastic process. At low temperatures and bias voltages, the differential conductance (dI/dV) is related to the density of electronic states. However, the electronic states of the junction, consisting of the metal tip, the substrate, and an adsorbed atom or molecule, are complex and the spectra are difficult to interpret. The problem is compounded by the fact that the electronic levels of adsorbed species are broadened into resonances and shifted due to many-body interactions with the substrate. Furthermore, electronic states of the adsorbed molecules are often located more than 2 eV from the Fermi level such that tunneling into these states require electrons with energies which might be sufficiently high to break chemical bonds.

The imaging capability is the bedrock of the STM, enabling direct visualization of the spatial distribution and the individual profiles of the adsorbed species. This allows a precise knowledge of the environment of each species and the selection of a particular species to study. The STM topographical images of a molecule can, however, be different from one substrate to another, making chemical and structural determination difficult, e.g., acetylene on Cu(001)

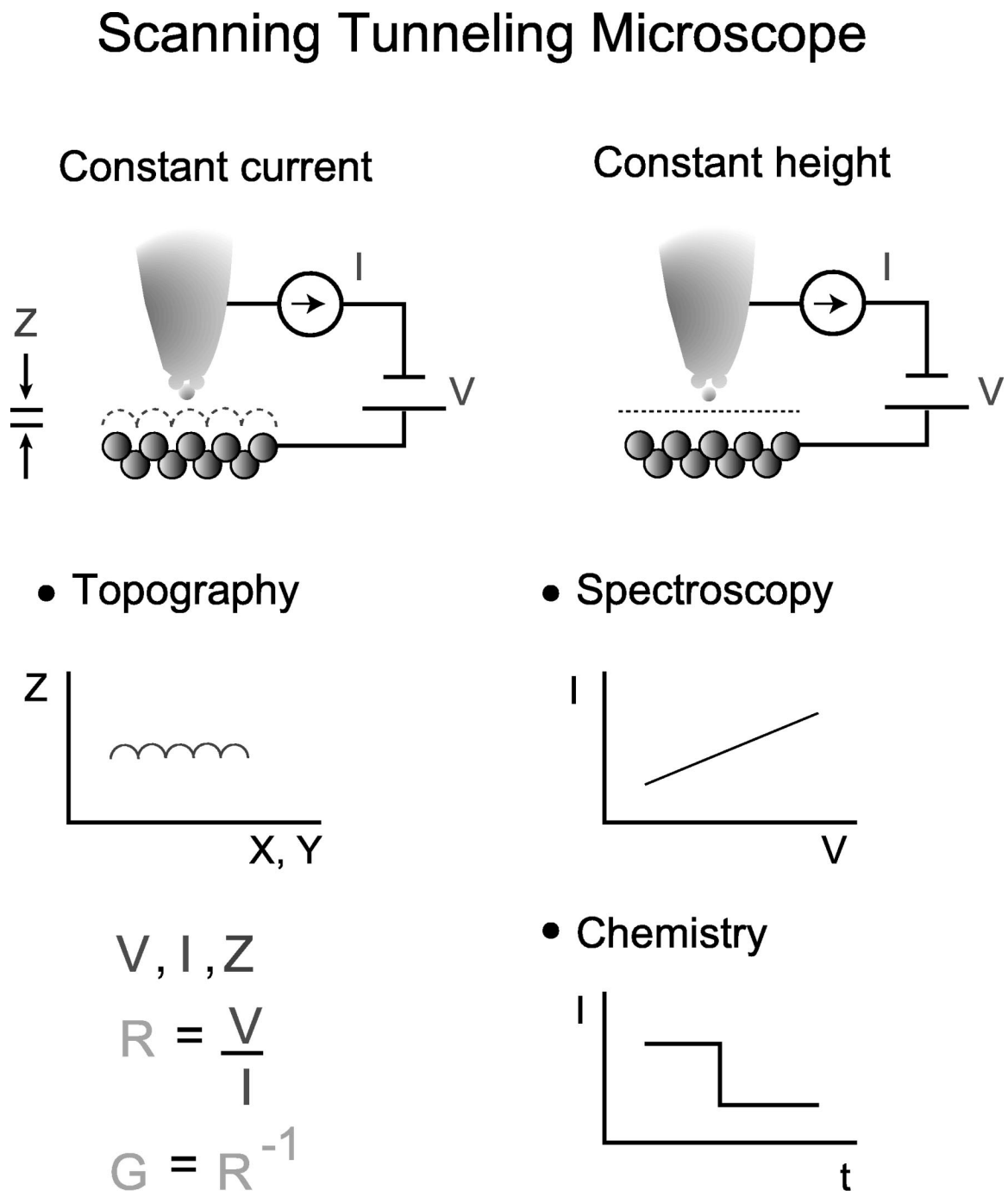

FIG. 2. Schematic showing the different operational modes of the STM. In the constant current (constant height) mode, the feedback remains on (off). With the tip fixed in the $x-y$ position and height (z), electronic and vibrational spectroscopy can be carried out by modulating and sweeping the bias voltage. By monitoring the time dependence of the current, motions of the molecule can be observed and quantitatively measured. With the homemade STM, the measured drifts with the feedback turned off are $\sim$0.001 Å/min for the tip–sample separation and $\sim$0.01 Å/min for the $x-y$ position. G is the conductance.

versus Ni(001).[102] This is because these images arise almost entirely from the elastic tunneling between the electronic structure of the tip, the molecule, and the surface. The interpretation of these images poses a great challenge for electronic structure calculations. Hidden in these images are the inelastic excitations, such as the vibrational excitations of the adsorbed molecule, which can be extracted spectroscopically. A great virtue of vibrational spectroscopy lies in the characteristic energies for the different functional groups. While the topographic images of acetylene on Cu and Ni surfaces show vast variations, the vibrational energies are nearly the same, suggesting that the bonding is similar on these surfaces.[102]

Vibrational spectroscopy with tunneling electrons was first demonstrated in 1966 by Jaklevic and Lambe from molecules adsorbed at the buried metal–oxide interface of a metal–oxide–metal tunneling junction.[103] Electrons tunneling through the $\sim$30 Å thick oxide were able to excite vibrational modes of the sandwiched molecules. While inelastic electron tunneling spectroscopy (IETS) is about 10 times as sensitive as other surface vibrational techniques, such as

electron energy loss spectroscopy (EELS) and infrared spectroscopy, as few as 10^9 molecules are required for a useful spectrum. Furthermore, the bonding structure and the environment of the buried molecules are not known and difficult to probe.

The STM provides a way to measure the ''topographical relief'' and the vibrational spectrum of the single molecule in the junction. We now have a tool that combines subangstrom spatial resolution and single-bond vibrational sensitivity.[77,104–106] From the characteristic vibrational energies, chemical identification of molecular species is possible and data analysis is much more straightforward compared to results which depend on the electronic states of the molecule–substrate system. STM-IETS is a threshold spectroscopic technique, as shown schematically in Fig. 3. When the sample bias is increased and crosses the threshold for excitation of a vibrational mode, the opening of the inelastic electron tunneling channel is accompanied by a change in the ac conductance (dI/dV). This change is more clearly detected by recording the differential change in the ac conductance as a function of the sample bias (d^2I/dV^2). The single bond sensitivity of STM-IETS is demonstrated in Fig. 4 where the topographic images of the three isotopes of acetylene are displayed with the corresponding single-molecule vibrational spectra.[102] While the images are indistinguishable between the three isotopes, the vibrational spectra clearly identify them. The single-bond sensitivity is shown by the two peaks observed for the C–H and C–D stretch vibrations of HCCD.

The spectra shown in Fig. 4 are striking in that only one mode, the C–H (C–D) stretch, is observed. There are emerging theoretical investigations which can explain the absence of other modes, namely the C–C stretch, C–H bend, and the vibration of the entire molecule against the surface.[107–109] The opening of the inelastic channel not only leads to an increase in the ac conductance but also influences the elastic tunneling, as shown schematically in Fig. 5. When the electron energy is near the threshold for excitation of a vibrational mode, electrons can directly tunnel elastically or through virtual de-excitation and excitation (or emission and absorption) of a vibrational quantum. These two pathways contain the same initial and final states and can thus interfere if they involve coherent processes. Excitation of a molecular vibration changes the density of states for elastic tunneling, and a decrease in the differential conductance of the elastic tunneling has been calculated.[108] The total measured conductance is the sum of the positive inelastic and the negative elastic contributions, which is nearly vanishing for all the modes except the C–H (C–D) stretch for acetylene on Cu(001), as shown in Fig. 4. This phenomenon is analogous to the Debye–Waller factor in the temperature reduction of the Bragg reflection intensities in x-ray, electron, and neutron diffractions.[110] As the temperature is increased, diffuse scattering becomes more prominent due to the increase in the likelihood of multiphonon excitations.[111] The emergence of these inelastic events leads to a reduction in the elastic diffraction intensities. In contrast to the involvement of many phonons, the reduction in the elastic conductance in STM-IETS is associated with the emergence of a single vibrational

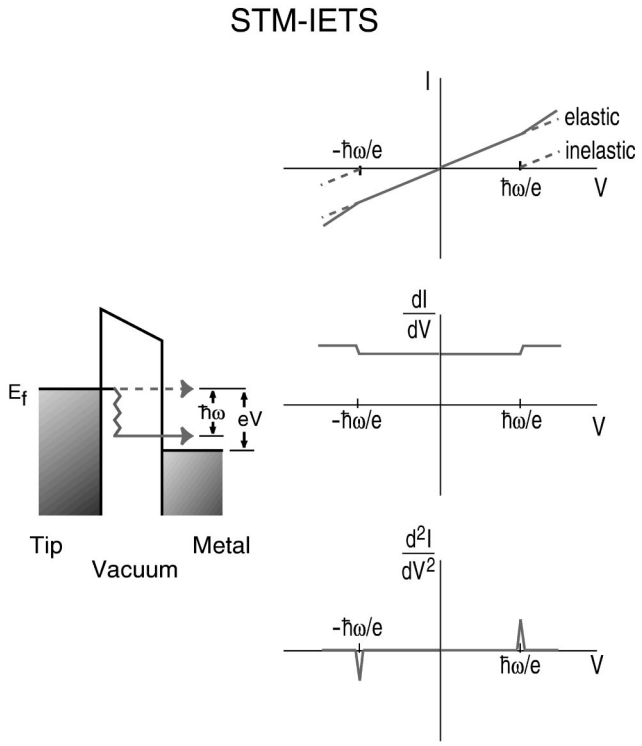

FIG. 3. Schematic showing the emergence of inelastic tunneling at the threshold for vibrational excitation. The change in the tunneling current due to vibrational excitation is too small to be measured from the $I-V$ curve. While a change in the differential conductance, dI/dV, can be seen for strong modes, more often vibrational features needs to be extracted from d^2I/dV^2. An important characteristic of vibrational inelastic electron tunneling spectroscopy (IETS) is the occurrence of a peak of the opposite sign on the negative bias side. Lacking an isotope shift analysis, the assignment of a feature to vibrational excitation needs to be confirmed by a corresponding feature with the opposite polarity at the opposite bias. This schematic depicts an increase in the conductance, associated with a positive (negative) peak for positive (negative) sample bias. In contrast, electronic spectra arise from elastic tunneling; peaks are positive and occur on either positive (unoccupied states) or negative (occupied states) sample bias.

excitation. Theoretical analysis of this phenomenon in STM-IETS together with the experimental data provide a novel way to probe the coupling of electrons to the nuclear motions, which is the basis for many chemical and biological processes.

The coupling of the elastic and the inelastic channels gives rise to different line shapes in STM-IETS. In addition to the positive peak observed for acetylene (Fig. 4), negative peaks are also possible, as in O_2 on Ag(110).[112] The line shape observed for the C–H stretch in pyrrolidine on Cu(001) has been determined to be due to the occurrence of negative differential resistance (NDR) at voltages across the threshold of the C–H stretch.[113,114] The NDR is manifested in a decrease in the current as the voltage is increased. This interesting, atomic scale $I-V$ relation has its origin in the dynamical coupling of the C–H stretch to a ring-buckling mode. The lack of vibrational features for some molecules, e.g., benzene on Cu(001),[115] provides us with additional insights into the mechanisms in STM-IETS. The adsorbed benzene has its plane parallel to the surface. Dehydrogenation by tunneling electrons caused the molecule to assume a nonhorizontal geometry from which C–H stretch was detected. The

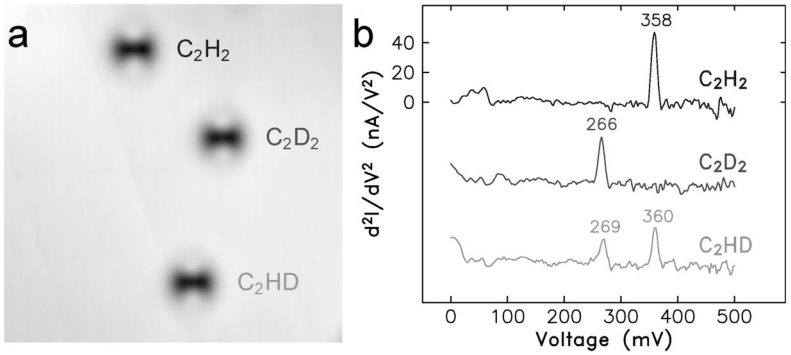

FIG. 4. (a) 56 Å×56 Å STM topographical images and (b) single-molecule vibrational spectra via STM-IETS of three acetylene isotopes on Cu(001) at 8 K. The two protrusions (bright) in the image of each isotope are due to the presence of the C–H and C–D bonds while the central depression (dark) is attributed to the C–C bond. The C–H stretch is observed at 358 meV for C_2H_2 and the C–D stretch is observed at 266 meV for C_2D_2. Small upshifts are found for the C–H and C–D stretches of C_2HD. The C_2HD spectrum demonstrated for the first time single bond sensitivity with STM-IETS.

four different line shapes observed to date are displayed in Fig. 6.

In macroscopic metal–oxide–metal tunnel junctions, the C–H stretch in hydrocarbons was the most prominent mode observed.[116] Taking that as a guide, the first successful IETS with the STM was obtained from acetylene on Cu(001).[77] The length of time to record the single-molecule vibrational spectrum of acetylene depends on the required signal to noise ratio. A peak is certainly discernable even after a single sweep of 24 s over a 100 meV range about the C–H stretch. To demonstrate the capability of long time averaging, data acquisition and tracking over a single molecule was carried out for 10 h over a 500 meV scan and compared to a spectrum averaged for 50 min.[77] Such capability enables signal averaging for weak intensity modes and for automatic overnight data acquisition.[77,104,105]

The C–H stretch has since been detected in a number of other single hydrocarbon molecules: ethynyl (C_2H, C_2D),[117] acetylene (C_2H_2, C_2D_2, C_2HD),[77,102] benzene (C_6H_6, C_6D_6),[115] pyridine (C_5H_5N, C_5D_5N),[115] pyrrolidine (C_4H_8NH, C_4D_8NH),[113] *N*-methylpyrrolidine ($C_4H_8NCH_3$),[114] tetrahydrothiophene (C_4H_8S),[118] and Cu(II) etioporphyrin-I on Cu(001);[119] acetylene (C_2H_2,

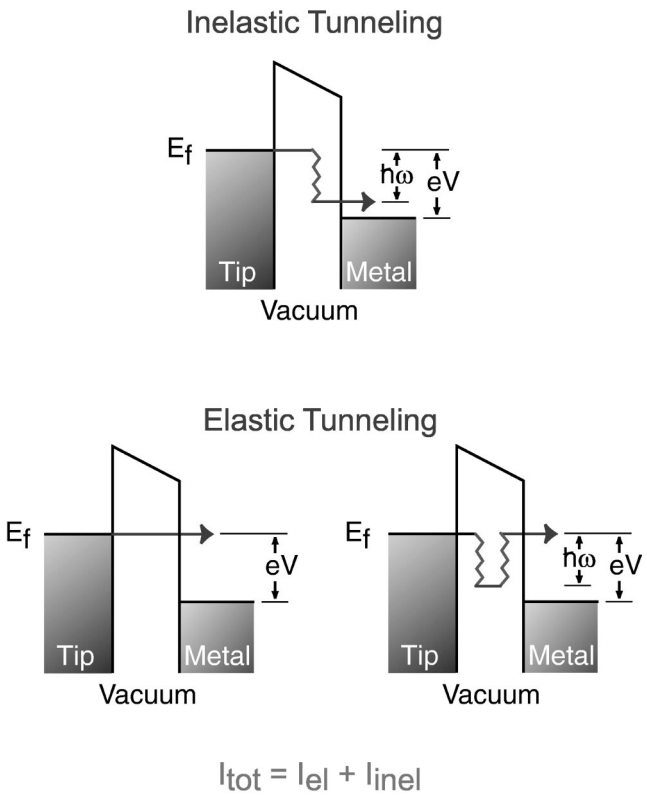

FIG. 5. Schematic diagram revealing inelastic tunneling and how the inelastic tunneling affects the elastic tunneling. The wiggly lines correspond to vibrational excitation. The elastic tunneling decreases at the threshold for excitation of a vibrational mode, leading to a decrease in the conductance. The inelastic tunneling always leads to an increase in the conductance due to the emergence of an additional channel (the inelastic channel) for tunneling. The total current measured is the sum of the elastic and inelastic tunneling. The net change in the conductance is similarly the sum of the changes in the elastic and inelastic conductance. These two have a canceling effect, accounting for the number and intensity of the observed vibrational modes.

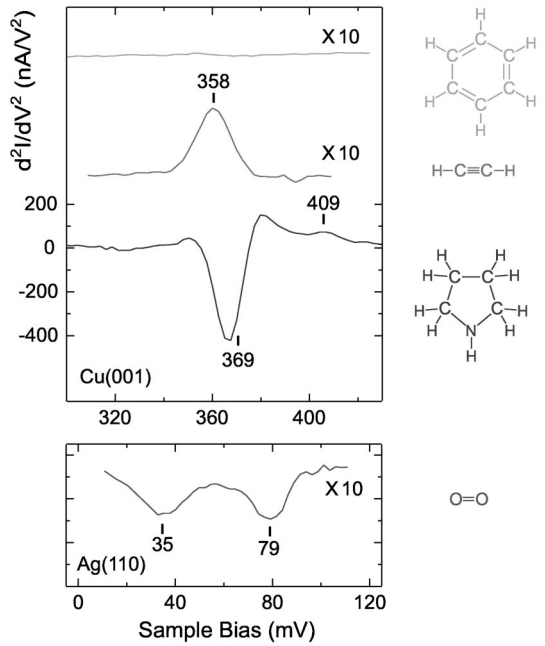

FIG. 6. Single-molecule vibrational spectra via STM-IETS for four different molecules, showing the variations in the intensity and line shape. Benzene, acetylene, and pyrrolidine are adsorbed on Cu(001) at 8 K while oxygen is adsorbed on Ag(110) at 13 K. The C–H stretch is observed at 358 meV and 369 meV for acetylene and pyrrolidine, respectively, while the 409 meV peak is attributed to the N–H stretch of pyrrolidine. The negative peaks at 35 meV and 79 meV are due to a hindered rotation (with motions of atoms perpendicular to the surface) and the O–O stretch, respectively, of O_2/Ag(110) with the O–O axis parallel to the surface. The lack of modes in benzene is correlated with the molecule bonded with its plane parallel to the surface.

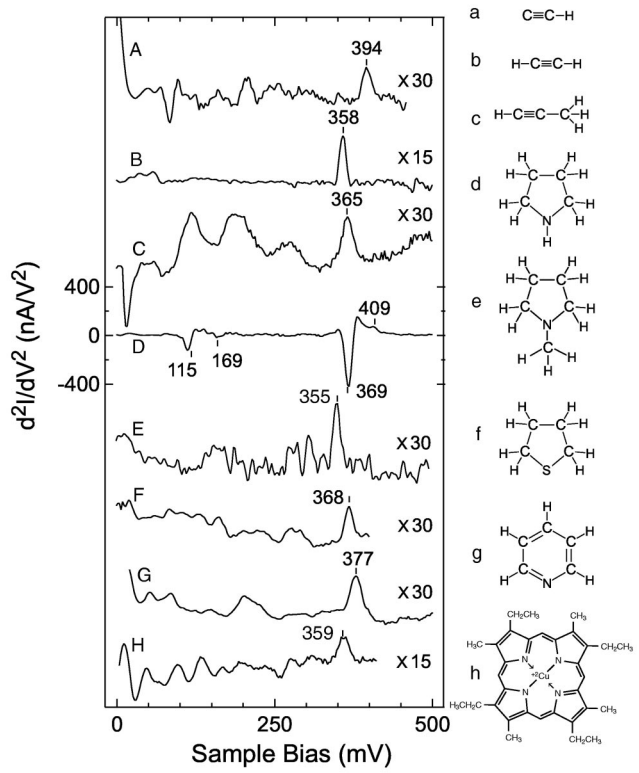

FIG. 7. A compilation of hydrocarbon molecules from which IETS spectra with one to four modes have been reported to date; the C–H stretch is the most prominent. Multiplicative factors in the spectra show the relative intensities from the different molecules. The spectra are offset for clarity of presentation.

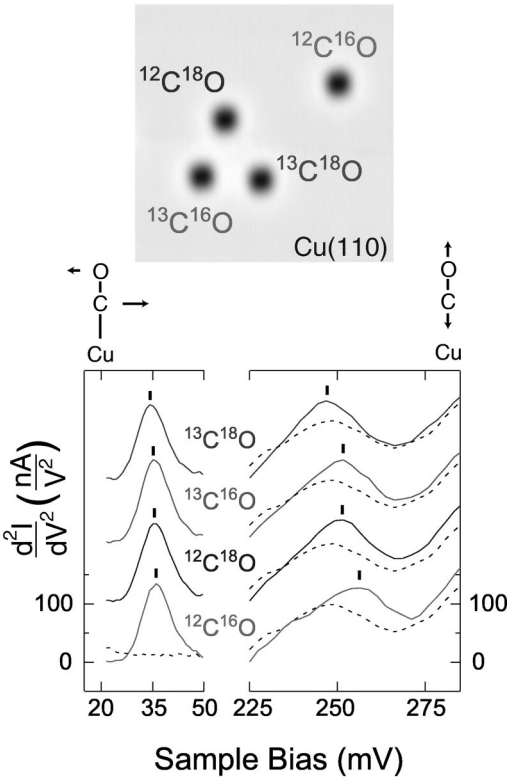

FIG. 8. The topographic image showing the four isotopes of CO adsorbed on Cu(110) at 8 K and the corresponding STM-IETS spectra revealing the C–O stretch and the CO hindered rotation.

C_2D_2, C_2HD) on Ni(100) (Ref. 102) and Ni(110),[120] propyne (CH_3CCH, CH_3CCD) on Ni(110);[121] pyridine (C_5H_5N) on Ag(110),[122] pyrrolidine (C_4H_8NH) on Ag(001).[118] For comparison, the single-molecule vibrational spectra of various hydrocarbons on Cu(001) recorded at ~10 K are gathered in Fig. 7. In the case of pyrrolidine, four modes are observed (N–H and C–H stretches, ring deformation, and CH_2 bending). Only one mode is observed for the other hydrocarbons (C–H stretch). Two modes (hindered rotation and C–O stretch) are observed for carbon monoxide ($^{12}C^{16}O$, $^{13}C^{16}O$, $^{12}C^{18}O$, $^{13}C^{18}O$) on Cu(001) and Cu(110),[123] as shown in Fig. 8. A hindered translational mode has also been tentatively assigned.[123] Similarly, two internal modes are resolved for oxygen ($^{16}O_2$, $^{18}O_2$; asymmetric stretch against the surface and O–O stretch) on Ag(110).[112] The vibration of the lightest element, hydrogen atom (H, D) against the Cu(001) surface demonstrates the ultimate sensitivity of STM-IETS.[124] One of the goals of STM-IETS is to expand on this list of adsorbate-substrate systems exhibiting ''tunneling active'' modes.

The strength and line shape of the STM-IETS features depend on the electron-vibrational coupling strength. Vibrational modes which show the largest relative changes in the differential conductance ($\Delta\sigma/\sigma$ exceeding 10%) are the C–H stretch mode in acetylene on Cu(001) (Refs. 77, 102) and the hindered rotational motion of CO on Cu(001) and Cu(110).[123] The detection limit for our STMs is $\Delta\sigma/\sigma \sim 0.3\%$. The detection of the C–O internal stretch requires a sensitivity $\Delta\sigma/\sigma \sim 1\%$.[123] While it is not yet possible to state the selection rules for STM-IETS, there are sufficient data to suggest that they are different from photon-based techniques, such as IR absorption and Raman scattering, and electron-based techniques, such as EELS. STM-IETS follows its own selection rules. By probing single molecules in well-defined environment, new observations are made which were not possible by probing more than 10^9 molecules in the macroscopic metal–oxide–metal planar tunneling junction. In addition, manipulation is precluded for molecules buried in the junction.

The high spatial resolution of STM-IETS enables the measurement of the energy, intensity, and line shape of vibrational features within a single molecule. The scanning capability of the STM makes it possible to obtain the spatial mapping of the vibrational intensity. In those cases where the vibrational modes are localized, vibrational microscopy can be used to locate specific chemical bonds. Localization occurs with isotopic substitution, as shown in Fig. 9, or when the two bonds are spatially separated, as in the case of Cu(II) etioporphyrin-I.[119] In addition to structural determination, these measurements are also valuable for the interpretation of the STM topographical images.[102] Vibrational microscopy provides information on the extremes in the changes of the ac conductance due to inelastic tunneling, which is useful in guiding the positioning of the tip for maximum signals in dI/dV and d^2I/dV^2.

Interest in STM-IETS is continuing to expand since the first measurement of single-molecule vibrational spectros-

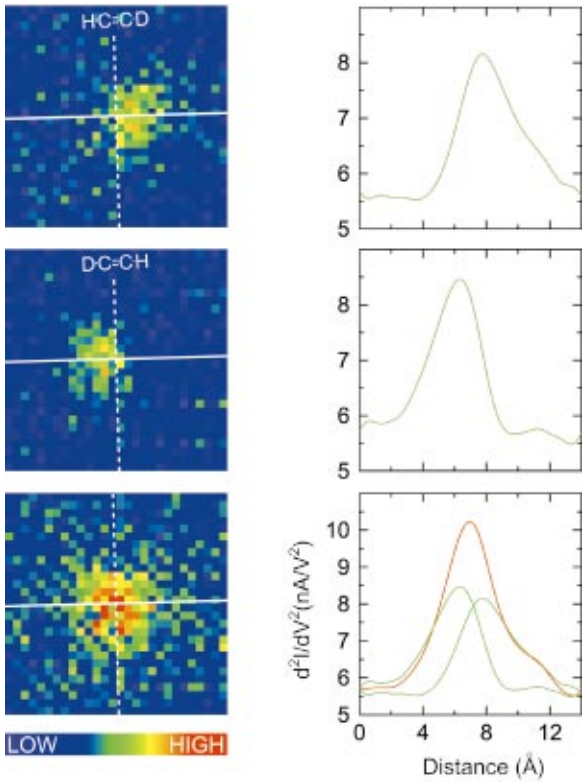

FIG. 9. (Color) Vibrational microscopy of the C–D stretch in the mixed isotope of acetylene (C_2HD) on Cu(001) at 9 K. The image is the d^2I/dV^2 signal at the voltage corresponding to the peak of the C–D stretch. The spatial localization of the C–D stretch intensity is demonstrated by rotating the molecule 180° and measuring the corresponding shift in the C–D stretch intensity distribution. The sum of the two C–D stretch intensity distributions is found to agree with the C–D stretch intensity distribution for C_2D_2. The right-hand column shows the cross sections taken along the solid lines in the d^2I/dV^2 images.

copy and microscopy in 1998.[77] The hindered translation and rotation of CO (Ref. 125) and the C–H stretch of acetylene[125] on Cu(001) as well as C_{60} (Ref. 126) and two unassigned vibrational modes of benzene on Ag(110) (Ref. 127) have been obtained with a 4 K-STM in the group of H.-P. Rust at the Fritz Haber Institute in Berlin. Using a tip terminated with a CO molecule, the hindered translation and rotation of CO on Cu(211) have been reported by K.H. Rieder's group at the Free University, Berlin.[128] The same two modes of CO have also been observed on Cu(111) by D.M. Eigler's group at IBM Almaden Research Laboratory.[129] It is worthy to note that most recently a commercial low temperature STM has been demonstrated to have the required stability and sensitivity to allow STM-IETS; the C–H stretch of a *trans*-2-butene molecule was detected by M. Kawai's group in RIKEN, Japan.[130] It is expected that the application of STM-IETS will continue to grow in both the range of problems and the number of research groups in the coming years.

IV. ROTATIONAL MOTIONS OF ISOLATED MOLECULES

Motions of atoms and molecules are an integral part of chemical transformation. While vibrational motions of adsorbed molecules have been probed extensively[131] by photons (infrared absorption, Raman scattering, and laser induced fluorescence), electrons [electron energy loss spectroscopy (EELS)], and neutrons (inelastic neutron scattering), the rotational motions have hardly been investigated. Most notably, rotational modes were observed by EELS for an ensemble of molecular hydrogen physically adsorbed at $\sim$10 K on Ag(111) and Ag films,[132] Cu(100),[133] highly ordered pyrolitic graphite,[134] and Cu(510).[135] The study of molecular hydrogen may provide insights into the dissociative chemisorption process as the molecular hydrogen may be the precursor to dissociation.

More recently, advancement made in single-molecule studies led to the direct observation of the rotational process, thus providing a new dimension to our understanding of this important motion. Laser induced fluorescence coupled with sample preparation technique have allowed real space visualization of the rotational motion of the γ-subunit of F1-ATPase.[1] Rotations of smaller molecules, down to a diatomic molecule, have been imaged with the STM. Excitation of the librational mode of the nearly parallel bonded O_2 molecule on Pt(111) led to the reversible, hindered rotation of the molecule on the surface.[136] By scanning the STM tip at a high bias voltage, reversible rotation of antimony dimers on Si(100) surface has also been observed.[137] Using a tracking technique, quantitative studies were made on the reversible rotation of individual Si ad-dimers on Si(100) surface.[138] Imaging different orientations of acetylene on Pd(111) provided evidence for its rotation on the surface.[139] While the above studies were made on isolated molecules, rotation of hexa-*tert*-butyl decacyclene on Cu(100) was observed when the molecule became unhindered from the neighboring molecules.[140] A change in the STM image from well defined set of protrusions to a uniform, averaged distribution was attributed to the rotational motion at room temperature. Low temperature experiments on isolated hexa-*tert*-butyl decacyclene on Cu(100) would provide support for this interpretation. It should be noted that, in contrast to free rotational motions for molecules in the gas phase, these single-molecule rotations correspond to hindered rotations where energetic barriers between stable sites are crossed in the rotational process.

A. Rotation induced by single and multiple tunneling electrons

The rotation of single O_2 molecule on Pt(111) was induced and monitored by tunneling electrons.[136] In addition to capturing the different orientations of the molecule, the moment of transition between them was measured with the feedback turned off (i.e., the gap distance is held fixed and the current changes as the molecule rotates underneath the tip; see Fig. 2). The distribution of time intervals between individual rotational events follows a simple exponential, implying that the probability of rotation per unit time is a constant and does not depend on the history of the molecule's orientation. The rotation rate is simply given by the inverse of the time constant of the exponential. By repeating the measurements at different sample bias voltage and initial tunneling current, quantitative understanding of the rota-

tional mechanism was obtained. The rotational rate showed various power dependencies on the tunneling current for different bias voltages, revealing a transition from single-electron to multi-electron process in overcoming the rotational barrier. The voltage at the transition yielded the energy for the barrier. These experiments illustrate a new application of the STM, allowing a quantitative measurement of the rates of fundamental molecular motions.

The single exponential distribution of the rotation rate is obtained for isolated single O_2 molecules. When the O_2 is in the vicinity of an impurity, defect, or another molecule, the rotation is significantly altered. The time distribution between rotational states is no longer exponentially distributed. The different orientations of the molecule are no longer equivalent and the molecule spends more time in one over the others. Such a behavior reflects a change in the potential energy surface for the O_2 molecule even though the STM image remains visually the same. These results point toward the importance of studying single molecules in a known environment, as can be characterized by the STM. Detailed theoretical calculations have been carried out on the rotation of O_2 on Pt(111).[141] The results are in good agreement with the data, thus providing a more rigorous understanding of the observed phenomenon.

B. Vibrational-rotational energy transfer

Materials transformations involve motions of individual atoms and molecules. In chemical reactions, the vibrational and rotational motions are often critically involved in the breaking and forming of individual bonds. The study of the coupling and relaxation of these motions is therefore central to a microscopic understanding of chemistry and materials.

The concept of the reaction coordinates hinges on the notion that motions of specific bonds dictate the progress of the reaction. Thus by selectively exciting these bonds, the rates and pathways of chemical reactions can be affected. Indeed bond-selected chemistry has been achieved in the gas phase.[142] In addition to selective deposition of energy into the reaction coordinates, it is necessary for the reaction to occur prior to the dissipation and randomization of the initially localized energy. Indeed this has been the bottleneck in the realization of bond-selected chemistry. By initiating the reaction with a femtosecond laser, fast reactions can be induced before the initial excitation is distributed to other lower energy states which no longer can lead to the desired reactions.[143]

Bond specificity has not been unambiguously demonstrated for reactions of molecules adsorbed on solid surfaces.[144] Although the energy is initially deposited into a specific vibrational mode of the molecule by infrared irradiation, rapid intramolecular and intermolecular relaxations occur in addition to substrate excitations. However, the use of femtosecond lasers has led to branching ratios of surface reactions which are different than those obtained with nanosecond lasers, indicating temporal control of the rates of energy distribution vs chemical reaction.[145]

In order to fully describe the dynamics of chemical reactions, it is necessary to understand the mechanisms and rates of vibrational relaxation and distribution. Time resolved measurements have shown that an important path for the decay of the $\upsilon(\mathrm{CH})$ stretch mode of liquid hydrocarbons is via the excitation of two $\delta(\mathrm{CH})$ bending modes.[146] In inert gas matrices, the stretching vibrations of simple hydrogenated molecules have been determined to couple efficiently to nearly free rotational modes.[147,148] For CO, the rotational motion is hindered and the energy in the $\upsilon(\mathrm{CO})$ stretch is transferred to the librational modes.[149] The relaxation of $\upsilon(\mathrm{CH})$ stretch in CH_3S adsorbed on Ag(111) has also been attributed to the excitation of $\delta(\mathrm{CH})$ bending modes.[150] Although the relaxation rates on semiconductor surfaces are generally smaller than on metal surfaces, the relaxation mechanism of the $\upsilon(\mathrm{SiH})$ stretch for H adsorbed on Si(111) involves the excitation of the $\delta(\mathrm{SiH})$ bending modes.[151] In condensed media, the discrepancy in energies between the stretch mode and the sum of the bending modes of the molecule can be absorbed in the low energy excitations of the media.

The number of modes increases in polyatomic molecules, allowing the possibility to probe different motions in a single molecule. Because of the imaging capability of the STM, it is possible not only to induce but view the motions of the molecule. The direct visualization gives certainty in the specific motion being analyzed.

Tunneling electrons were used to induce and monitor the hindered rotational motion of single acetylene molecule adsorbed on Cu(001) at 8 K.[152] The molecule rotates between two orientations, as shown in Fig. 10. As in the case of O_2 rotation on Pt(111),[136] the moment of rotation from one orientation to the other is evidenced by a stepwise change in the current. The rate of rotation per electron at each bias voltage is given by the inverse of the time constant in the exponential distribution of the rotation times. The rotational rate was observed to increase significantly (50-fold) at the threshold of the $\upsilon(\mathrm{CH})$ stretch in C_2H_2 and shows a 20-fold increase and an isotopic shift to the $\upsilon(\mathrm{CD})$ stretch in C_2D_2, as shown in Fig. 11. The coupling of the stretch vibration to the rotational motion in single adsorbed molecule is believed to occur via the simultaneous excitations of the bending vibrations and substrate states (electron–hole pairs and phonons). The probability of rotation per C–H or C–D excitation is $\sim 1\times 10^{-8}$. Taking the probability of C–H or C–D vibrational excitation to be $\sim$1%, we can conclude that the probability for rotation per electron is $\sim 1\times 10^{-10}$ or a rate of 1 rotation per second for $\sim$1 nA of tunneling current and a bias voltage above the C–H or C–D vibrational excitation. By studying the motions of an isolated molecule, additional effects due to intermolecular interactions and relaxation are eliminated.

C. Chemically sensitive rotation

The voltage dependence of the rotation rate per electron, shown in Fig. 11, provides a new way to characterize bonding in a molecule by analyzing its rotational motion. In the mixed isotope of acetylene, C_2HD, the C–H and C–D bonds certainly can be distinguished by their vibrational energies. By choosing the bias voltage between those corresponding to

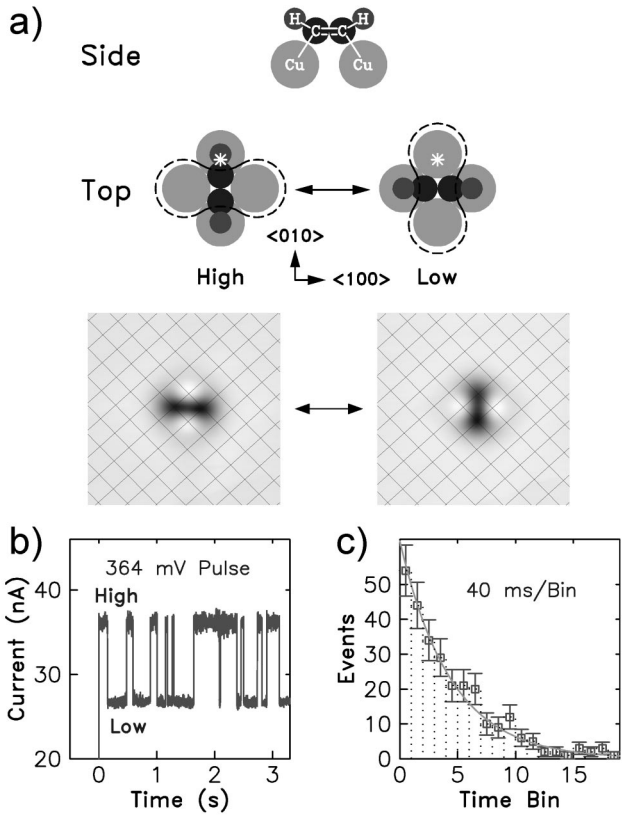

FIG. 10. (a) Schematic drawing of acetylene on Cu(001) showing side and top views. The dashed line represents the outline of the dumbbell shaped depression in STM images. The asterisk shows the position of the tip over the molecule for measuring the rotational rates. The square lattice in the STM images represents Cu atoms of the substrate, determined from an atomic resolution of the same area with a C_2H_2 molecule adsorbed on the tip. (b) Current during a 364 mV voltage pulse over a C_2H_2 molecule initially in the high current orientation. Each jump in the current indicates the moment of rotation of the molecule. (c) Distribution of the times the molecule spent in the high current orientation with a fit to an exponential decay. The fitted time constant is 184 ms for the voltage and current in (b). [B.C. Stipe, M.A. Rezaei, and W. Ho, Phys. Rev. Lett. **81**, 1263 (1998).]

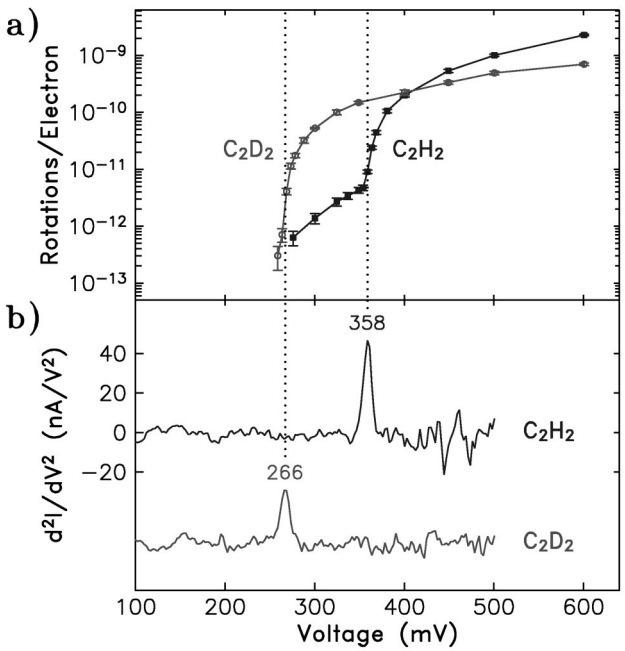

FIG. 11. (a) Rotations per electron for C_2H_2 and C_2D_2 on Cu(001) at 8 K as a function of sample bias voltage. (b) d^2I/dV^2 spectra for C_2H_2 and C_2D_2 show C–H and C–D stretch vibrations. Each spectrum is an average over four voltage ramps of 2 min each.

the C–D and C–H stretch energies, 266 meV and 358 meV, these two bonds can be spatially located and the slight difference in bond lengths can be measured.[102]

In Fig. 12, the rotational motion of C_2HD is induced and monitored by setting the bias voltage at 300 mV and the tip at a fixed height above a chosen point in the molecule. When the D is below the tip, the rotational rate is faster than when the H is below the tip since 300 meV is above the C–D stretch energy but below the C–H stretch energy. Furthermore, from the current versus time trace, the current is 0.7 nA lower for D versus H, suggesting that the C–D bond is shorter than the C–H bond or the wave function for C–D is tighter than that of C–H. Since the tunneling current is exponentially dependent on the tip–sample distance, a height differential of 0.007 Å is deduced from the analysis of individual rotational events between C–H and C–D ends of the molecule.

A single exponential distribution in the time intervals between rotational events is observed for the low current level, corresponding to the orientation of the molecule with the tip outside the molecular plane. In contrast, the time intervals for the high current level exhibit a double exponential distribution with the faster (slower) decay associated with the time intervals when the D(H) is below the tip. Thus the rotational motion allows distinction between the two ends of the single C_2HD molecule.[102]

V. THERMALLY INDUCED ROTATION AND DIFFUSION

The study of the thermal diffusion and rotation of molecules on solid surfaces is central to our understanding of

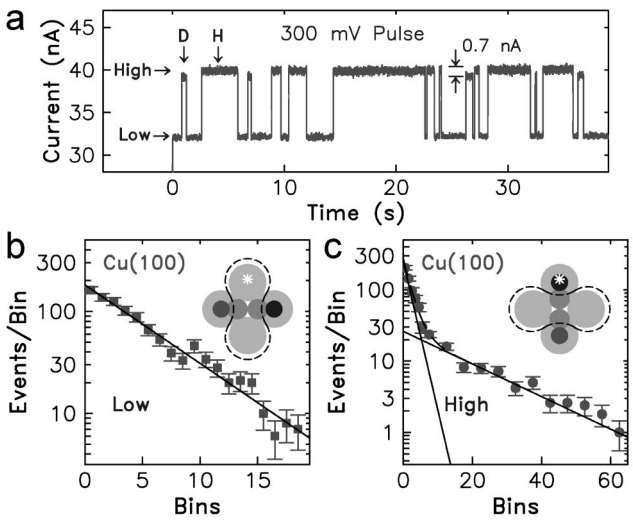

FIG. 12. (a) Current during a 300 mV voltage pulse over the C_2HD molecule on Cu(001) at 8 K. Distribution of rotation times are shown for the low (b) and high (c) current states. In the schematic insets, the position of the tip is marked with an asterisk while the depression part in the STM images is outlined. The bin width is 100 ms.

how chemical reactions proceed on the atomic scale. Thermal excitations may provide the energy necessary for reactants to diffuse to active sites and upon arrival, surmount an energy barrier to reaction. Reaction barriers can depend on molecular orientation as well as the degree of rotational excitation. Chemical reactions are often modeled as trajectories of molecules on potential energy surfaces, and measurements of the energetic barriers related to the translational and rotational motions provide both input for and testing of theoretical calculations. The microscopic parameters which determine macroscopic reaction rates are ideally measured at the molecular level.

Significant contributions to the understanding of surface diffusion at the atomic scale have been made with field ion microscopy (FIM).[153] The surface area of the microscope tip, however, is limited and edge effects on diffusion need to be considered. Additionally, rotational motions are difficult to probe and a new preparation of the surface is required after field-induced desorption to record an image.

An understanding of the rotational motion also cannot be obtained by probing the behavior of an ensemble of molecules. Laser induced fluorescence (LIF) detected through an optical microscope was used successfully to monitor the rotational motion within a single enzyme molecule, thus providing a microscopic mechanism of energy transmission for the enzyme.[1] Similarly, direct observation has been made of the translational motion of a motor protein along a microtubule[154] and the diffusion of individual lipid molecules in membranes[155] and protein molecules in water-based jels.[156] This laser-based approach provides a molecular basis for unraveling the connections between motions and functions in biological systems. In contrast to FIM, atomic resolution is not obtained in LIF.

Recent advances in scanning tunneling microscopy (STM) has made it possible to probe both the diffusion and the rotational motion of a single molecule. While most measurements have been on small molecules, from which detailed understanding has been obtained,[102,136,152] there is no fundamental limitations to its applications to large molecules, albeit at reduced spatial resolution.[140]

The classic method for studying diffusion and rotation (and also chemistry) with the STM is that of repeated imaging to take snapshots of the on-going surface processes. The positions, orientations, and chemical states of a number of molecules are monitored on a frame-by-frame basis until a significant number of events are recorded. The accuracy of this approach is limited by the scanning time to acquire an image. An important consideration in these experiments is the ability to vary the temperature to match the time scales of molecular processes to the data acquisition speed. Using this approach, the thermal rotation and diffusion of C_2H_2 on Pd(111) were captured; activation barriers for rotation and diffusion were measured based on an assumed pre-exponential factor.[139]

A variable temperature STM in the single-molecule tracking mode allows fast and quantitative measurements to be made on the thermally induced rotation and diffusion rates of a single acetylene on Cu(100) between 68 K and 208 K,[157] and the rotation rates of ethynyl between 27 K and 36 K.[158] Similar approach has been used to measure the thermal diffusion[159] and rotation[138] of Si ad-dimers on Si(100). These studies complement those made on nonthermally induced rotation by tunneling electrons for antimony dimers on Si(100),[137] oxygen on Pt(111),[136] and acetylene on Cu(100).[102,152] The prevalence of thermally induced reactions makes it desirable to understand the different motions which are thermally excited.

Rotational motions induced and monitored by tunneling electrons provide insights into molecular properties such as intramolecular vibrational relaxation (IVR), molecular structure, nonlinear induction, and intermolecular interactions. However, only in some cases, such as the rotation of O_2 on Pt(111),[136] the energy of the rotational barrier can be deduced from the bias voltage at which transition from linear to nonlinear current dependence of the rotational rates is observed. In contrast, by assuming an Arrhenius behavior, activation energy and pre-exponential factor can be obtained from the temperature dependence of the rate. Such measurements require a variable temperature STM and the proper match of the temperature range to the rate of data acquisition.

The thermally induced rotation of single-molecule acetylene (C_2H_2) was monitored over the temperature range 68 K to 94 K on Cu(001).[157] Similar to rotation induced by tunneling electrons, each rotational transition is monitored by a rapid change in the current. The Arrhenius plot is shown in Fig. 13, yielding an activation energy of 169 ± 3 meV and a pre-exponential factor of $10^{11.8\pm0.2}$ s^{-1}. The corresponding values for C_2D_2 are 168 ± 4 meV and $10^{11.7\pm0.2}$ s^{-1}. The use of rotational motion for chemical identification is illustrated by the differences between acetylene (C_2H_2, C_2D_2) and ethynyl (CCH, CCD) on Cu(001). The rotation rates of ethynyl were found to be significantly higher than those for acetylene.[158] The activation energy and pre-exponential factor for CCH and CCD are: $E_H=56.2\pm0.5$ meV, $\nu_H=10^{11.0\pm0.1}$ s^{-1}; $E_D=56.8\pm0.5$ meV, $\nu_D=10^{10.9\pm0.1}$ s^{-1}. The rotational energy barriers are approximately three times smaller than acetylene. Since ethynyl was produced by the dehydrogenation of acetylene,[117] the rotational motions of the reactant and product can be used for chemical identification at the single-molecule level. This is particularly useful since the C–H (C–D) vibrational intensity is very weak for CCH (CCD) even though a large upshift of 38 meV (48 meV) was observed for the C–H (C–D) stretch compared to that for C_2H_2 (C_2D_2).[117] In addition to the time dependent current trace, the rapid rotation in ethynyl leads to a distinct topographic image characterized by streaks and fuzziness due to the rotation when the tip is scanned over the molecule.

The acetylene molecules start to diffuse on Cu(001) at temperatures above 178 K.[157] An Arrhenius plot of the diffusion rate over the temperature range of 178 K to 208 K is shown in Fig. 14, revealing an activation energy and pre-exponential factor of $E_H=0.53\pm0.01$ eV, $\nu_H=10^{13.6\pm0.2}$ s^{-1}. The energy barrier for diffusion is close to three times larger than the rotational barrier. While the rotational motion was monitored between 68 K to 94 K, extrapolation to $\sim$200 K yields a rotation rate of $\sim10^6$ s^{-1}. A detailed picture of the motional dynamics is thus obtained. As

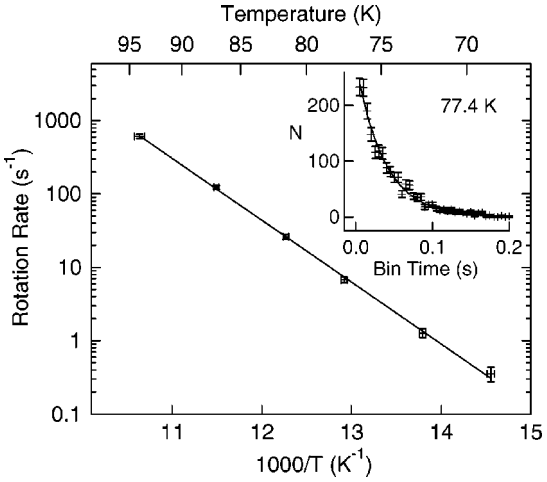

FIG. 13. Arrhenius plot of the logarithm of the rotation rate vs $1000/T$ for C_2H_2 on Cu(001). The data are fit to $R=\nu\exp(-E_a/kT)$. The inset shows the number of rotations N observed at 77.4 K as a function of the time between rotations, grouped into 5 ms time bins. The distribution is fit by a single exponential and the inverse of the time constant yields the rotation rate at that temperature. [L.J. Lauhon and W. Ho, J. Chem. Phys. **111**, 5633 (1999).]

the acetylene molecule is diffusing on the surface, it is rotating at a very fast rate, analogous to the motion of a helicopter moving on a two-dimensional lattice. The ability to obtain such understanding into the fundamental motions of a molecule illustrates the unique capabilities of the STM in the study of single molecules.

VI. DIFFUSION BY QUANTUM TUNNELING

The phenomenon of quantum tunneling for particle motions is most readily observable for the lightest element, the hydrogen atom. Diffusion of hydrogen atoms on metal surfaces has been investigated quite extensively because of its relevance in many chemical processes and being a favorite system for theoretical analysis. Pioneering measurements were carried out by field emission microcopy (FEM).[160–163] Subsequent studies were made by helium atom scattering[164] and various optical techniques.[165–167] A major problem in these experiments lies in probing and averaging over the behavior of a large number of hydrogen atoms. Thus the nature of the low temperature diffusion observed on Ni and W surfaces remains unclear due to difficulties arising from the possible effects of steps, defects, and adsorbate–adsorbate interactions, as well as difficulties in establishing absolute values for the diffusion rate.[163] Substantial disagreements are found between experimental methods, including the actual existence of a temperature independent regime on Ni(111).[162,167] One outstanding puzzle is the unexpected small difference in H and D diffusion rates in nonactivated regime measured by FEM.[162,163] These measurements of the low temperature diffusion are in qualitative disagreement with theoretical work where transitions to quantum diffusion have been found.[168–172]

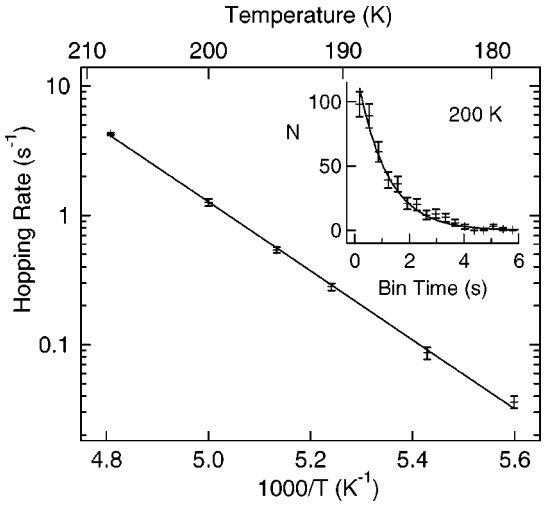

FIG. 14. Arrhenius plot of the logarithm of the hopping rate vs $1000/T$ for C_2H_2 on Cu(001). The data are fit to $R=\nu\exp(-E_a/kT)$. The inset shows the number of hops N observed at 200 K as a function of the time between hops, grouped into 150 ms time bins. The distribution is fit by a single exponential and the inverse of the time constant yields the hopping rate at that temperature. [L.J. Lauhon and W. Ho, J. Chem. Phys. **111**, 5633 (1999).]

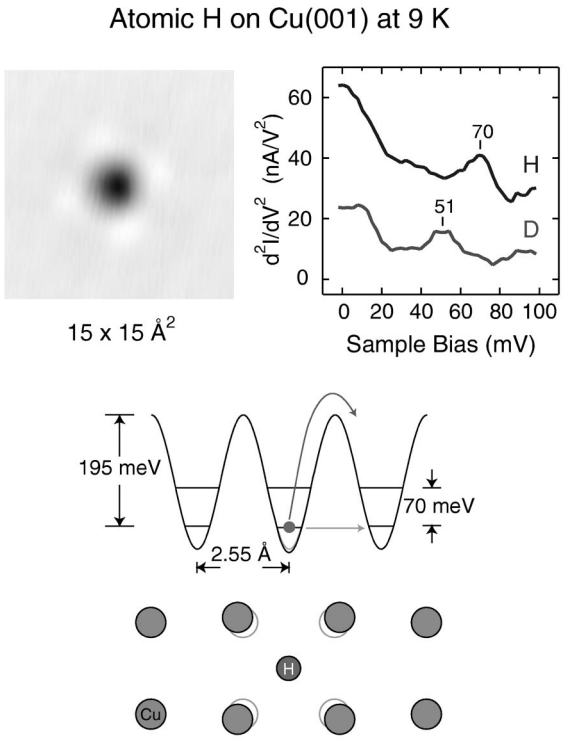

FIG. 15. STM image, 15 Å×15 Å, of an isolated hydrogen atom on Cu(001) at 9 K. STM-IETS spectra of H and D showing the H–Cu and D–Cu stretch mode. Signal averaging times were 14 and 28 min for these H and D spectra, respectively. Schematic diagram showing the fourfold hollow adsorption site and the slight distortions of the underlying Cu substrate atoms to lower the overall adsorption energy. The diffusion barrier is 195 meV.

The effect of a surface impurity or coadsorbed molecule on the rotational motion was quantitatively measured for O_2 on Pt(111).[136] Similar perturbations on the diffusion of hydrogen atoms were observed on Cu(001).[124,173] The nature of the diffusion is changed when two hydrogen atoms are close to each other. Diffusion occurs as a pair rather than as individuals; the motion of one affects the motion of the other. These STM experiments bring to light the importance of

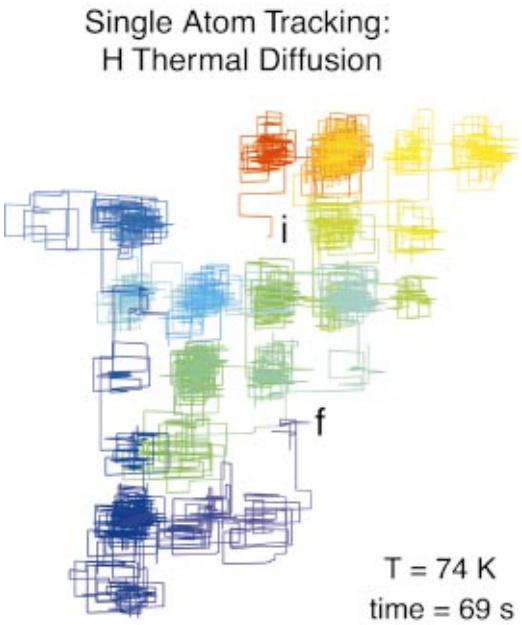

FIG. 16. (Color) Tip positions showing the tracking of single H thermal diffusion on Cu(001) at 74 K, starting from the initial position (i) and ending in the final position (f) in 69 s. The progress of the time sequence of the random walk is mapped to the spectrum of the rainbow color. Each concentration of tip positions indicates a H atom in a given lattice site. The denseness of each concentration is directly proportional to the residence time. A plot of the binning of residence times follows an exponential distribution, and the inverse of the time constant of this distribution yields the hopping rate at this temperature.

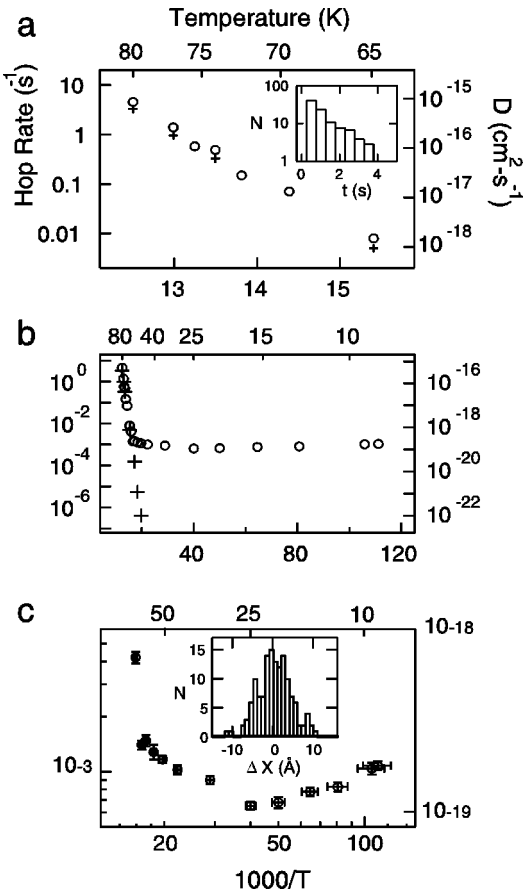

FIG. 17. Classical and quantum diffusion of H and D on Cu(001). (a) Arrhenius plot of the hopping rate of H (○) and D (+) atoms determined by single-atom tracking between 65 K and 80 K. The right axis gives the equivalent single particle diffusion constant, D, which is related to the hopping frequency ν by $D=1/4l^2\nu$, where the lattice constant $l=2.55$ Å. The inset shows an examplary histogram of 130 residence times for a H atom in the fourfold hollow site at 77 K. (b) Arrhenius plot of the hopping rate of H (○) and D (+) between 80 K and 9 K. measured by single-atom tracking (80 K–65 K) and repeated imaging (63 K–9 K). (c) Log–log plot of the H hopping rate between 63 K and 9 K. The inset shows the individually measured diffusion lengths of 140 H atoms along an arbitrary x-axis over 3 h at 25 K.

single-molecule studies where the environment is precisely known.

Hydrogen has been extensively studied on semiconductor surfaces, but the large potential corrugations lead to significant barriers to surface diffusion.[174,175] To date, hydrogen atoms have only been imaged on the Cu(001) surface at low temperatures.[124] A topographic image of an isolated hydrogen atom is shown in Fig. 15. STM-IETS was used to unambiguously determine that the depression in the image is indeed a hydrogen atom. The vibrational energy of 70 meV corresponds to a hydrogen atom adsorbed on a fourfold hollow site and vibrating perpendicular to the surface. The downshift of this vibrational peak to 51 meV for a deuterium atom confirms the assignment of this mode. The fourfold symmetry of the weak protrusions surrounding the depression in the STM image supports the adsorption site for the atoms.

The diffusion of hydrogen corresponds to hopping from site to site on the square lattice of Cu(001) surface with nearest neighbor distance of 2.55 Å. From an Arrhenius plot of the thermal diffusion rate (shown in Fig. 17), a barrier of 195 meV is deduced and the vibrational levels within the potential, with spacing of 70 meV for H, is provided by STM-IETS. Diffusion can be either thermally activated by overcoming the barrier or by quantum tunneling through the barrier, as shown in Fig. 15.

Between 80 K and 65 K, diffusion of H and D atoms can be followed by an atom-tracking technique which was similarly used to follow the thermal diffusion of individual acetylene molecules.[157] The hopping between nearest neighbor sites is shown in Fig. 16. The fourfold symmetry of the Cu(001) lattice is apparent. During the tracking process, the tip scans eight points in a circle with the feedback on and their average positions is recorded. If the atom moves to a nearest neighbor site, a gradient is sensed from the changed tunneling gap distances. The tip then moves in the direction of the gradient by a preset amount and a new average of the eight points is obtained and is the new position of the tip. Figure 16 is a plot of the tip positions during the tracking process. For temperatures above 80 K, the diffusion rate is too fast to be followed by the tracking technique. Below 65 K, the opposite problem occurs, and it becomes increasingly likely for the tip to influence the atom due to prolonged interactions.

Repeated imaging of a chosen area of the surface was used to monitor the diffusion of H and D below 65 K. By keeping track of the locations and the environment of ~100 atoms every ~15 min over the course of several hours, the distances traveled by these atoms were measured. The hop-

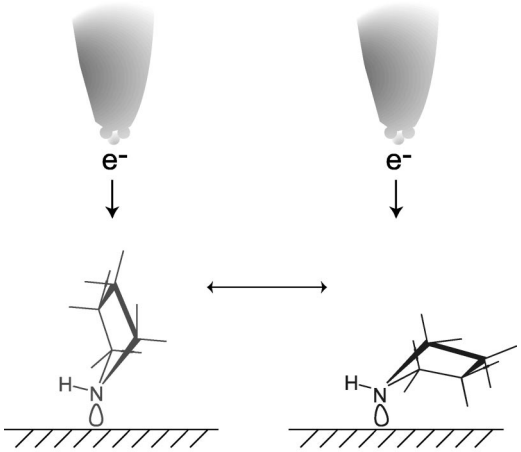

FIG. 18. Schematic diagram showing the conformational change of pyrrolidine-h_9 induced by tunneling electrons with the tip fixed in position.

ping rates were obtained for H and D, as shown in Fig. 17. It is apparent that below 60 K, the rate of H diffusion abruptly levels off while the rate of D diffusion continues to decrease exponentially. At the lowest temperature of 50 K measured for D, the thermal hopping rate is 4×10^{-7} s^{-7}, or one hop every 29 days for a D atom. It can be seen that D has not reached the regime of quantum tunneling. From the rates shown in Fig. 17, the tunneling probability for D is at least three orders of magnitude lower than for H, consistent with a factor of 5×10^5 calculated for H and D on Ni(001) (Ref. 169) and Cu(001).[176]

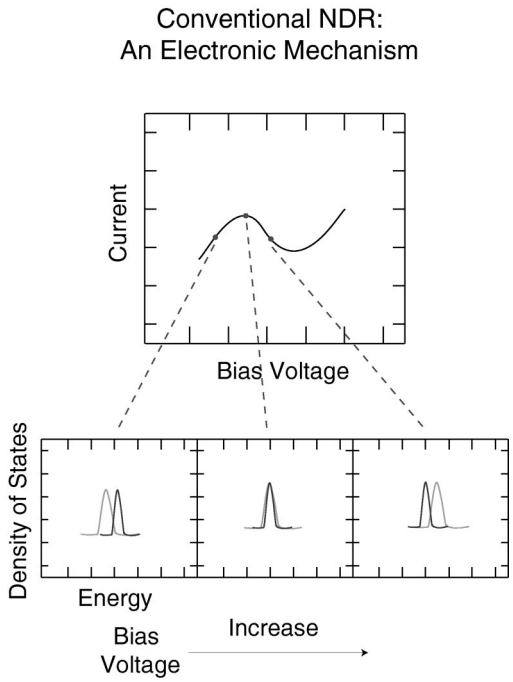

FIG. 20. Schematic diagram showing the origin of the electronic mechanism of the conventional NDR effect. As the bias voltage increases, an electronic state sweeps through another electronic state in the conducting media, causing the current to first rise, reaching a maximum, and then decrease. The maximum in the current corresponds to the maximum overlap between the two electronic states.

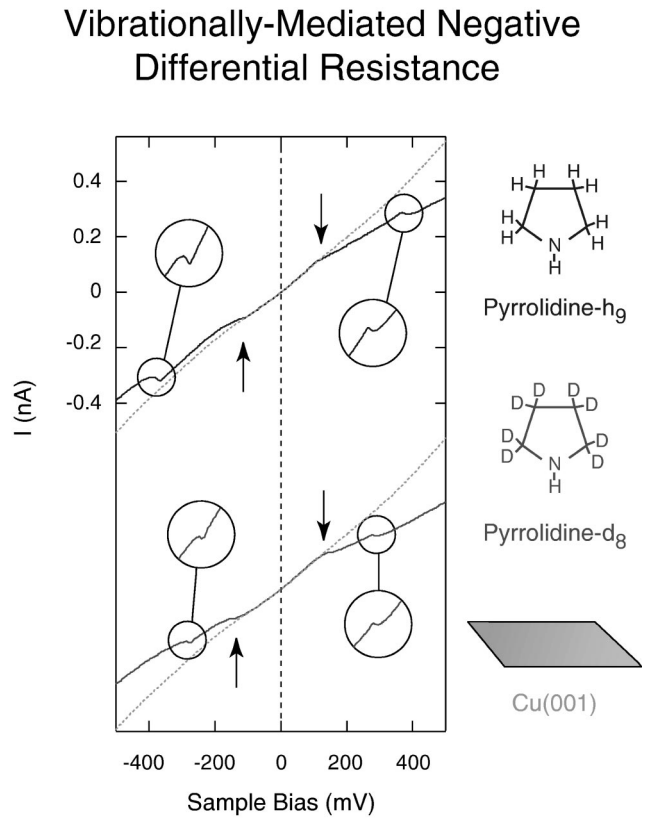

FIG. 19. $I-V$ curves for pyrrolidine-h_9 (upper curve), pyrrolidine-d_8 (lower curve), and over the clean Cu(001) at 9 K (dashed line). The lower curves are offset for clarity. Expanded views (×6) of the NDR regions; arrows indicate the additional nonlinear sections of the $I-V$ curves. The voltages at which NDR occur correspond to C–H and C–D stretch vibrations.

A close examination of the quantum tunneling rate reveals that the rate is not a constant but decreases first between 65 K and 25 K and then increases below 25 K. Above 25 K, the data are consistent with phonon assisted tunneling. Below 25 K, the increase in rate is due to the decrease in nonadiabatic response of the thermally excited electron–hole pairs to the diffusing particle. Similar phonon-assisted and electron-limited tunneling processes have been observed for muons, protons, and deuterons in bulk metals, insulators, and superconductors.[177–179]

The schematic diagram of the potential energy wells shown in Fig. 15 suggest that diffusion should be enhanced if the hydrogen atom is in a vibrationally excited state. Thus the coupling of vibration to diffusion provides insights into intramolecular energy transfer similar to the coupling of vibration to rotation in acetylene on Cu(001).[152] Excitation of the C–O stretch has been shown to lead to enhanced diffusion of CO on Pd(110).[180]

VII. CONFORMATIONAL CHANGE: VIBRATIONALLY MEDIATED NEGATIVE DIFFERENTIAL RESISTANCE

One of the important applications of STM is that it enables direct measurement and visualization of intramolecular vibrational relaxation (IVR) in a single molecule. These experiments require monitoring time-dependent changes in the

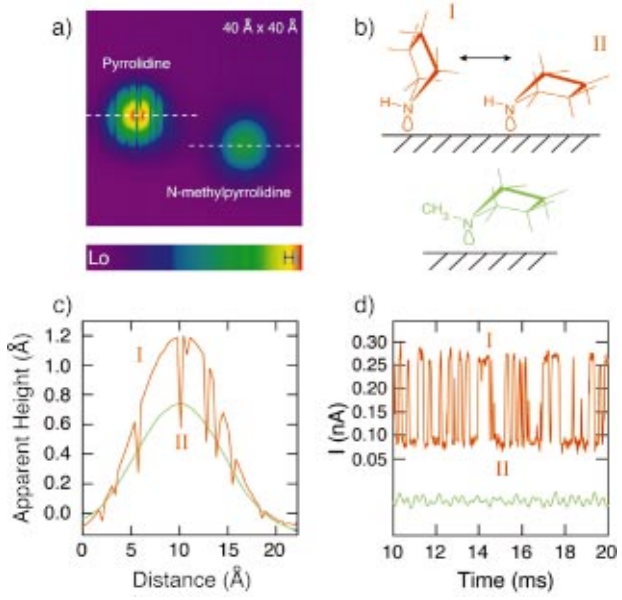

FIG. 21. (Color) (a) 40 Å×40 Å topographic image of pyrrolidine and *N*-methylpyrrolidine on Cu(001) at 9 K. The pyrrolidine flipped between two states (I and II) as the tip was scanned across the molecule, whereas *N*-methylpyrrolidine did not change (scanning conditions: 50 pA and 30 mV). (b) Schematic picture of the two proposed conformations of adsorbed pyrrolidine (top) and single conformation of *N*-methylpyrrolidine (bottom). (c) Cross sections of pyrrolidine (red) and *N*-methylpyrrolidine (green) images, taken along the dashed lines in (a). (d) Current collected during a voltage pulse with the sample bias corresponding to 16 meV above the CD_2 (CH_2) stretching energy of pyrrolidine-d_8 (*N*-methylpyrrolidine). Two current levels corresponding to states I and II are seen in the pyrrolidine-d_8 (red) current trace; only one current level is observed for *N*-methylpyrrolidine (green), with an average current value of 0.14 nA (for clarity the current trace for *N*-methylpyrrolidine is offset). [J. Gaudioso and W. Ho, Angew. Chem. Int. Ed. Engl. **40**, 4080 (2001).]

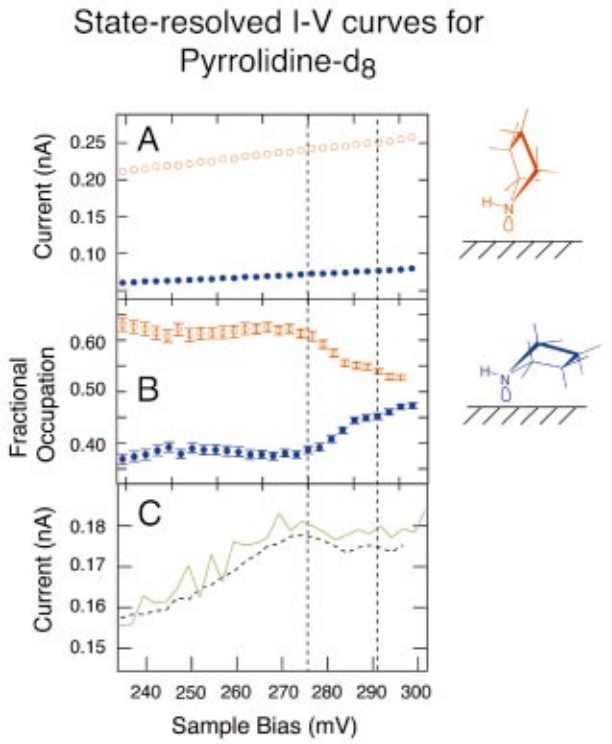

FIG. 22. (Color) (A) State-resolved $I-V$ curves on pyrrolidine-d_8 [State I (○), State II (●)] determined from current traces as in Fig. 21(d). (B) Fractional occupation as a function of bias for the two states of pyrrolidine-d_8. The vertical dashed lines show the range of biases where NDR was observed, as can be seen from Fig. 19. (C) State-averaged $I-V$ on pyrrolidine-d_8 (solid line) and the simulated $I-V$ curve (dashed line). The simulated $I-V$ curve is obtained from multiplying curves in (A) and (B) and summing the two contributions. [J. Gaudioso, L.J. Lauhon, and W. Ho, Phys. Rev. Lett. **85**, 1918 (2000).]

current level and correlating the observed behavior at different sample bias voltages with single-molecule vibrational spectra obtained by STM-IETS.

The relaxation of the high energy C–H (C–D) stretch vibration to lower energy modes of the molecule and the substrate leads to excitation of other degrees of freedom in the molecule. Thus IVR has led to enhanced rotation[152] and diffusion[180] in a single molecule. Similarly, conformational changes have been affected, leading to the observation of negative differential resistance in a single molecule.[113,114] Pyrrolidine on Cu(001) undergoes a structural change analogous to the boat-chair conformational transformation in cyclohexane, as shown in Fig. 18. With the tip stationary above the molecule (feedback turned off), two levels of the tunneling current are measured, corresponding to the two conformations of the molecule. The high (low) current level is obtained from the ''upright'' (''parallel'') configuration.

In the $I-V$ curves measured for pyrrolidine-h_9, negative differential resistance (NDR) was observed across the C–H stretch vibration, as shown in Fig. 19. The association of the NDR with vibrational excitation was confirmed with the NDR observed across the C–D stretch vibration in pyrrolidine-d_8. These experiments discovered a vibrationally mediated mechanism for the NDR which is qualitatively different than that for all other NDR systems which can be attributed to electron transport involving discrete states in the electronic structure, as illustrated schematically in Fig. 20. For systems with restricted dimensions, there can be present discrete states, e.g., in superlattices with few atomic layers in each lattice. As the voltage increases, the electronic level in one part of the system sweeps across another electronic level in another part. The amount of current flowing through the system is directly proportional to the overlap for the two electronic levels.

In vibrationally mediated NDR, the occurrence of the nonlinear $I-V$ curves is due to an interplay among vibrational excitation, IVR, and energy lost to the substrate. From the time-dependent current, each occurrence of the conformational change is monitored, as shown in Fig. 21. From the time intervals in the high current state (conformation I or ''straight'' conformation) and the low current state (conformation II or ''parallel'' conformation), the fractional time spent in each conformation can be obtained as a function of the sample bias voltage, as can be seen in Fig. 22. Even though the $I-V$ curve for each conformation is a linearly increasing function, the fractional time spent in conformation I (II) decreases (increases) as the sample bias voltage increases across the C–D stretch vibration (pyrrolidine-d_8 is analyzed due to the slower transformation rate). The current due to both conformations, i.e., the tunneling current that is measured in Fig. 19, is the weighted sum of the current in

each state times the fractional occupation of that state. NDR in the $I-V$ curves is reproduced from this state-resolved analysis. In fact, in addition to finding a new mechanism for NDR, these results demonstrate the feasibility of state-resolved experiments at the single-molecule level. Population analysis was carried out for each conformation of the molecule as a function of the excitation energy of the tunneling electrons which induce the conformational transformation.

The ''parallel'' conformation becomes increasingly favorable as the bias voltage increases across the threshold for C–D vibrational excitation (similar results apply to the C–H vibration in pyrroline-h_9). Figure 18 shows that the tip–molecule separation is smaller for the ''upright'' conformation than the ''parallel'' conformation. The probability for C–D vibrational excitation is thus higher for the ''upright'' conformation, leading to a higher rate for IVR and in particular energy transfer into the ring deformation mode. Since the conformational transformation involves the ring deformation mode, excitation of the C–D stretch leads to the transition from the ''upright'' to the ''parallel'' conformation. Similar IVR occurs for the ''parallel'' conformation. However, the tip–molecule separation is larger, leading to correspondingly smaller C–D stretch excitation probability and IVR rate. Furthermore, the ''parallel'' molecule is closer to the surface, which enhances energy coupling to the substrate in the form of phonon and electron–hole pairs excitation. This energy loss channel into the substrate takes away the internal energy in the molecule that could be used for conformational transformation. The enhancement of conformational transition across the C–D stretch vibration combined with the more efficient loss of energy to the substrate favor the ''parallel'' conformation which corresponds to the low current state. Thus as the bias voltage increases across the C–D vibrational excitation, the sum of the currents from the two conformations is weighted increasingly toward the ''parallel'' conformation, thus dragging down the average current that is measured to give the NDR effect.

The association of the NDR effect with the transformation between the two conformations is further confirmed with the substitution of a methyl group for the hydrogen attached to the nitrogen atom in pyrrolidine, as illustrated in Fig. 21. The transformation is sterically hindered by the more bulky methyl group in *N*-methylpyrrolidine. The current remains steady as a function of time and the STM image does not display the streakiness that is characteristic of the conformational changes in pyrrolidine. Distinct differences have also been obtained in the STM-IETS spectra for the two molecules.[114] Whereas four modes are observed for pyrrolidine, only the C–H (C–D) stretch mode is resolved for *N*-methylpyrrolidine.[114]

VIII. BOND DISSOCIATION: UNIMOLECULAR REACTION

Vibration, rotation, translation, and conformation changes are basic molecular motions which can be uniquely investigated by the STM. These motions are responsible for inducing chemical transformations that require nuclear motions. In the dissociation of a chemical bond, excitation energy is ultimately converted into moving atoms apart. It remains a challenge to decipher the pathway and to determine the identity of the reactants, intermediates, and products in a chemical reaction. By studying the dissociation of single molecules, the STM enables a new way to understand the

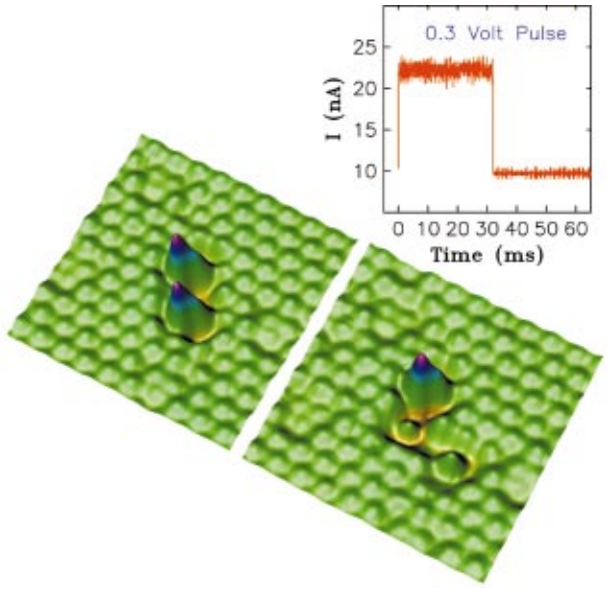

FIG. 23. (Color) Three-dimensional topographic image showing the dissociation of one of the two O_2 molecules to form two O atoms on Pt(111) at 40 K by positioning the tip over the chosen O_2 molecule. The other O_2 molecule remains unperturbed. Individual Pt atoms are resolved. Inset shows the current trace. The sharp drop in current at ~30 ms corresponds to the moment of dissociation of the O_2 molecule for 0.3 V bias and ~22 nA tunneling current.

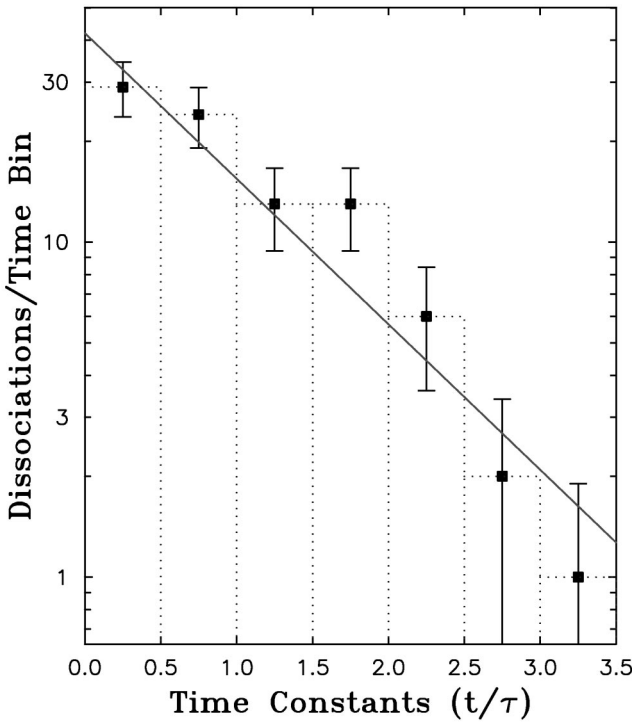

FIG. 24. The distribution time for dissociation at fixed bias voltage and tunneling current, showing the single exponential dependence. For an exponential distribution, the average time is the same as the time constant of the exponential function.

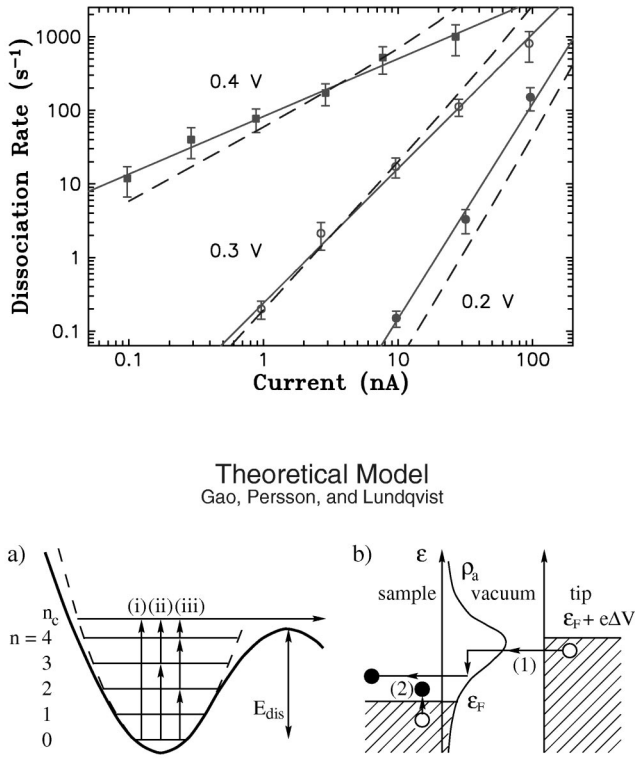

FIG. 25. Dissociation rate, R_d, of O_2 on Pt(111) at 40 K as a function of tunneling current for various sample bias voltages. The solid lines are least squares fits to the data and correspond to power laws, $R_d \sim I^N$, where $N = 0.8 \pm 0.2$, 1.8 ± 0.2, and 2.9 ± 0.3 for sample biases of 0.4, 0.3, and 0.2 V with respect to the tip, respectively. Results from theoretical model are shown with dashed lines and have corresponding exponents of $N = 1.17$, 2.07, and 3.13, respectively. (a) Schematic diagram of the model for bond breaking via the ladder climbing mechanism. Potential energy well (solid line) for the intramolecular bond coordinate is modeled by a truncated harmonic oscillator (dashed line). The three sets of excitations among the levels represent typical transitions that lead to dissociation for (i) 0.4 V, (ii) 0.3 V, and (iii) 0.2 V. (b) Inelastic electron tunneling to an adsorbate-induced resonance with density of states ρ_a induces vibrational excitations, (1), while electronic excitations within the substrate induces vibrational relaxation (2). [B.C. Stipe, M.A. Rezaei, W. Ho, S. Gao, M. Persson, and B.I. Lundqvist, Phys. Rev. Lett. **78**, 4410 (1997).]

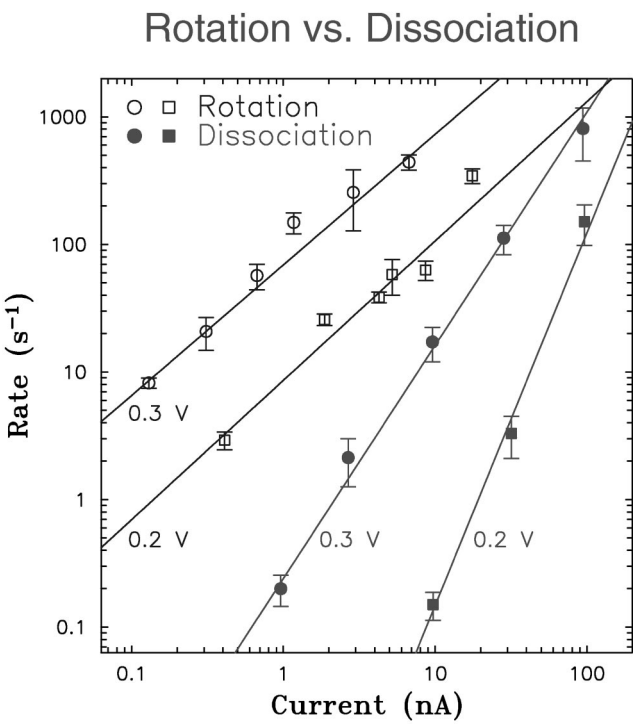

FIG. 26. Comparison of the rotation and dissociation rates of single O_2 on Pt(111) at 8 K as a function of the tunneling current for 0.2 V and 0.3 V sample bias.

process through the coupling of the electronic and nuclear degrees of freedom, spatially resolved spectroscopy, and direct visualization of the reactants and products.

A. Vibrational ladder climbing: Dissociation of O_2 on Pt(111)

A homonuclear diatomic molecule provides an opportunity to probe in detail the bond dissociation process due to the limited degrees of freedom. Oxygen adsorbs molecularly on Pt(111) below 95 K. Three different types of O_2 adsorption sites were observed on this triangular surface: bridge, threefold hollow, and at steps. Dissociation of individual oxygen molecules adsorbed on the threefold hollow site was probed in detail because it can be more easily found isolated on the surface.[181] In addition, tunneling electrons can be used to induce and monitor the rotation of this type of oxygen molecule.[136]

Figure 23 shows two oxygen molecules adsorbed on the nearest neighbor threefold hollow sites. The two molecules can be dissociated one at a time by positioning the tip over the chosen molecule and subjecting it to a pulse of electrons. The resulting two-oxygen atoms are imaged, showing the distance they have traveled and their occupation of two different threefold hollow sites (the fcc and hcp sites, with or without a Pt atom below in the second layer). The electron induced dissociation has produced a nonequilibrium oxygen atom since only oxygen atoms on the fcc threefold hollow sites are present from thermal dissociation of oxygen molecules.[182] Since ~1 eV/atom of energy is released, the separation of the two oxygen atoms by 1–3 lattice constants suggests an efficient quenching by the substrate. From the current trace, as shown in Fig. 23, the moment of dissociation at a given bias voltage and current (0.3 V and 22 nA), with the feedback turned off, can be obtained (~30 ms) to yield the dissociation rate. By repeating the measurement on many individual molecules, the distribution of dissociation times follows a simple exponential, as shown in Fig. 24 and consistent with the expectation that the probability for dissociation per unit time is a constant.

The energy barrier for the dissociation of oxygen in the threefold hollow site is 0.35–0.38 eV. A bias voltage of 0.4 V provides sufficiently high energy electrons to overcome the dissociation barrier in a one-electron step, as shown in Fig. 25. In comparison, at 0.3 V bias, a two-electron process is required. Due to the quantized nature of the vibrational states, a three-electron process is observed for 0.2 V bias even though two-electron process provides the required energy. At these voltages, the dissociation rate is experimentally observed to follow $I^{0.8 \pm 0.2}$, $I^{1.8 \pm 0.2}$, and $I^{2.9 \pm 0.3}$ for bias voltages 0.4 V, 0.3 V, and 0.2 V,[181] consistent with the one-,

two-, and three-electron process. The dissociation pathway takes the minimum number of steps in overcoming the energy barrier, a consequence of the balance between the excitation rate (arrival rate of the electrons at the molecule) and the vibrational relaxation rate. The tunneling electrons excite the molecular vibrations via being captured temporarily in a negative ion resonance as they traverse the molecule. This vibrational ladder climbing mechanism is generally behind reactions induced by heat, photons, or electrons.[183] The STM studies on single-molecule dissociation eliminates environmental effects such as interactions with other adsorbed molecules, defects, impurities, and steps on the surface, which lead to uncertainties when an ensemble of molecules is considered.

The study of single-molecule dissociation by the STM makes it possible to assess the relevance of different motions on the dissociation process. In the case of oxygen adsorbed on the threefold hollow site of Pt(111), molecules do not diffuse on the surface at temperatures below 95 K. Thus translational motion is not coupled to bond dissociation of O_2. However, the tunneling electrons used to induce dissociation are also efficient in rotating the molecule. In fact, rotation is facile under the conditions where dissociation may occur, as shown in Fig. 26. These results suggest that the molecule is rotating while it is being excited for dissociation. The angular motion could couple to the intramolecular vibrational motion of the molecule. Energy exchange may occur. A full theoretical analysis needs to take into consideration these different motions in the molecule and the potential energy surface necessarily becomes multidimensional. These results also point out the importance of measuring the rotational motion of a molecule, a property which has only been described quantitatively and observed visually by the STM.

B. Orbital specific chemistry

The dissociation of single oxygen molecule on Ag(110) illustrates another unique application of the STM. By changing the polarity of the sample bias voltage, electrons can either tunnel into or out of an electronic state of the molecule. In the case of O_2 on Ag(110), a π^* resonance is located at the Fermi level. Most strikingly, different products are formed for positive and negative bias, as illustrated in Fig. 27.[184] With positive bias, electrons are injected from the tip into the molecule. In contrast, electrons are removed from the molecule and flow to the tip with a negative bias on the sample. The threshold for dissociation is -390 meV and $+470$ meV for negative and positive bias, respectively.

The two oxygen atoms always are produced along the [110] direction, separated by one to three fourfold hollow sites, when the sample bias is positive, i.e., an electron is injected into the π^* orbital of the O_2 molecule. From the initial adsorption geometry, the O_2 molecule needs to undergo a rotational motion during the dissociation process in order for the two O atoms to be aligned along the [110] direction. In contrast, with negative bias, an electron is removed from the π^* orbital and the two oxygen atoms are produced and separated with substantially larger distance along the [001] direction (on the average ~10 Å larger than atomic separation obtained with positive bias). Furthermore, a new oxygen atom species is produced and is bonded on the short bridge site, which has previously not been documented. In thermally induced dissociation of O_2 molecules on Ag(110), the oxygen atoms occupy only the fourfold hollow sites. This bridge-O species has unusual properties. The bridge-O can be moved on the surface by tunneling electrons, jumping from site to site along and between rows of Ag atoms, but always occupying the short bridge sites. Even though it is thermodynamically less stable than the O atom in the fourfold hollow site (since it is not produced thermally), it cannot be induced by tunneling electrons to transfer to a fourfold hollow site. There appears to be present an energy barrier separating the short-bridge and fourfold hollow sites. As the bridge-O hops between rows, it manages not to fall into the fourfold hollow site in between the rows.

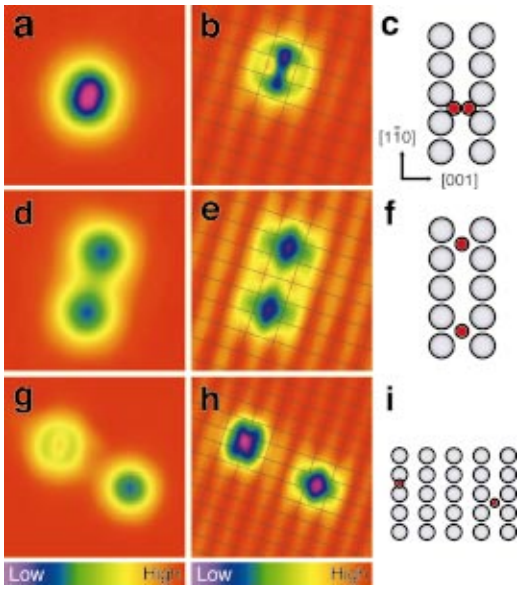

FIG. 27. (Color) Dissociation of O_2 chemisorbed on Ag(110) at 13 K. Images on the left column (a,d,g) are topographical images taken with a bare tip. Images at the central column (b,e,h) are obtained with a CO-terminated tip, showing atomic resolution of the substrate and the O_2 π^* orbital perpendicular to the surface. Grid lines are drawn through the Ag surface atoms. Schematic of the adsorption sites are shown on the right column (c,f,i). The scan area of the images in (a,b) is 25 Å×25 Å. Oxygen atoms dissociated along the [110] direction by +480 mV voltage pulse. The scanned area in (d,e) is 25 Å×25 Å. Oxygen atoms are produced along the [001] direction by a −390 mV voltage pulse. One oxygen atom is adsorbed on the fourfold hollow site and the other is adsorbed on the short bridge site. The scanned area in (g,h) is 31 Å×31 Å.

By choosing the sign and magnitude of the sample bias voltage, control of reaction pathway and product formation has been achieved with the STM inducing the dissociation of single molecules. In the case of O_2 on Ag(110), the difference in dissociation between positive and negative bias is completely reproducible for more than 100 molecules.

C. Dissociation by electronic excitation

In the case of hydrocarbons (ethylene, acetylene, benzene, pyridine), the dissociation requires significantly higher bias voltages (1–4 eV) compared to the fraction of an electronvolt for O_2 on Pt(111) and Ag(110). This is due to the

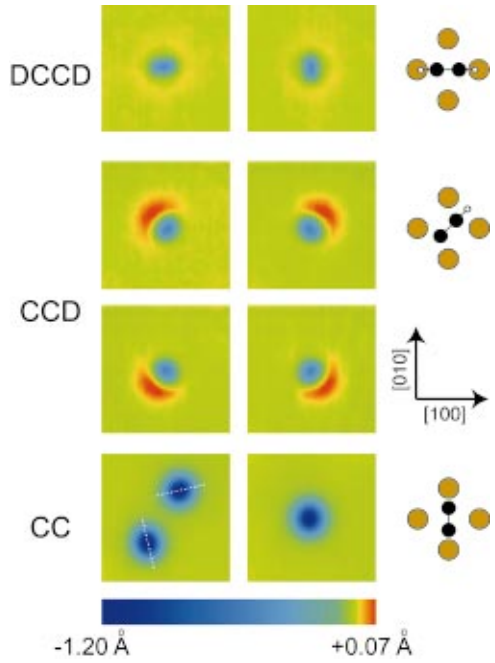

FIG. 28. (Color) 38 Å×38 Å constant current images of DCCD, CCD, and CC on Cu(001) at 9 K. All possible observed orientations of these molecules on fourfold hollow sites are shown. The directions of the Cu[100] and Cu[010] axes are indicated by the dashed white lines on the CC images and are rotated 20° with respect to those of the other images. Schematics of the molecular orientation are shown for one of the orientations for DCCD, CCD, and CC. The scale of the schematics is enlarged 5× with respect to the images. [L.J. Lauhon and W. Ho, Phys. Rev. Lett. **84**, 1527 (2000).]

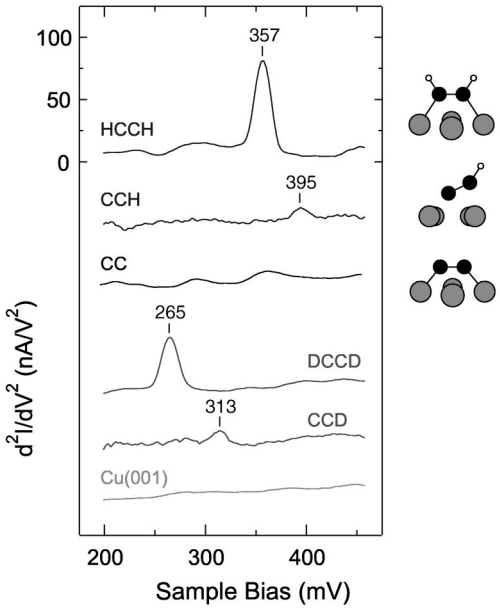

FIG. 29. Vibrational spectra of acetylene and ethynyl isotopes compared to those of CC and the bare Cu(001) surface at 9 K. The peak positions are indicated in meV. The peak intensity of the particular CCH chosen for signal averaging was anomalously low. With the same tip, the intensity ratio of ~1.4 for HCCH/DCCD also holds for CCH/CCD. [L.J. Lauhon and W. Ho, Phys. Rev. Lett. **84**, 1527 (2000).]

higher C–H bond energy and the lack of appropriate electronic resonances near the Fermi level. The stepwise dehydrogenation of ethylene to dicarbon species revealed a wealth of information on the mechanism and the nature of the intermediate species.[115,117,120]

In the dehydrogenation of different isotopes of ethylene to acetylene on Ni(110) at 13 K, the ethylene molecule hops away and returns to the original site repeatedly before it dissociates.[120] The observation of this process reveals a diffusional motions that a molecule executes during a chemical transformation. In addition, the C–H bonds are broken first to form deuterated acetylene with voltages in the range 1.1–1.5 V. The acetylene products were identified by STM-IETS. Dissociation of acetylene required higher voltages in the range 1.0–4.8 V.[120]

A stepwise dehydrogenation was observed for acetylene (C_2H_2, C_2D_2) on Cu(001) at 9 K.[117] The ethynyl intermediate (CCH, CCD) was characterized by its topographic image, rotational motion, and vibrational spectra. The threshold energy for the dissociation of the first C–H (C–D) bond in C_2H_2 (C_2D_2) is 2.8 eV (3.8 eV). Lower threshold energy of 2.1 eV (2.7 eV) is needed for the dissociation of CCH (CCD) to form CC. The topographic images for the acetylene, ethynyl, and dicarbon are shown in Fig. 28. While acetylene can rotate between two orientations, the reduced symmetry for ethynyl gives rise to its rotation among four equivalent orientations. The barrier for rotation is significantly reduced from acetylene to ethynyl (169 meV to 56 meV) while the barrier for CC rotation is much higher and its rotation was not observed.[158] From the symmetry of the STM topographical images, along with rotational and vibrational analyses, the adsorption structure for these three species can be determined. These results indicate that the plane of the molecule undergoes 45° rotations as the acetylene molecule undergoes stepwise dehydrogenation. The power of STM-IETS for chemical identification is illustrated in Fig. 29. The C–H (C–D) stretch vibration differs significantly between acetylene and the ethynyl intermediate.[117]

The threshold energy for the initial dehydrogenation of benzene is 2.9 eV (4.4 eV) for C_6H_6 (C_6D_6) and in the case of pyridine, 3.0 eV (3.2 eV) for C_5H_5N (C_5D_5N).[115] An up shift of 3 meV was observed in the C–H stretch of the dehydrogenated species. From the symmetry of the STM topographic images, it was possible to conclude a slight tilt in the molecular plane due to the inequivalent bonding of the C and the N of the pyridine ring to the surface. In the case of benzene, no vibrational feature was observed. However, the C–H (C–D) stretch vibration became tunneling-active when the molecule changes its orientation from ''parallel to the surface'' to ''upright'' after the first dehydrogenation. Unlike pyridine, the STM topographic images for benzene and its dehydrogenated product do not show the asymmetry observed for pyridine, consistent with the equivalent bonding of the two C atoms of the benzene ring to the surface.

As the molecule increases in size, it becomes more difficult to decipher the number of C–H bonds (or C–C bonds) which have been dissociated as further dehydrogenation takes place. The STM images do change with each dehydrogenation, but they are difficult to interpret. Together with STM-IETS, some qualitative understanding can be extracted from a combined analysis.

IX. SINGLE BOND FORMATION: BIMOLECULAR REACTIONS

The formation of chemical bonds presents a greater experimental challenge. By using sufficiently high voltage and current, a single molecule can be induced to undergo dissociation unless it hops away or desorbs from the surface. In order to form a chemical bond, the two reactants need to be brought close to each other and be the ''right type'' for each other. These two requirements, close proximity and chemical compatibility, underlie the challenges inherent in bimolecular reactions. Thus the study of single bond formation with the STM requires controlling the distance separating the two reactants and stimulation of the reaction. How close is close? By measuring the vibrational spectra to extract energy shifts, intensity changes, and line shape variations for different separations between two adsorbed molecules, it is possible to address the question on how close the two molecules need to be in order for them to affect each other and for a reaction to occur. These intermolecular induced changes provide unique insights into the nature of chemical interactions and the elastic and inelastic couplings of electrons with the molecular vibrations. Since electron tunneling involves the overlap of electronic wave functions of the tip, molecule, and the substrate, the STM is uniquely positioned to reveal the inner workings of molecules.

By combining the different attributes of the STM, reactants can be imaged, manipulated, spectroscopically characterized, and stimulated. The study of bimolecular reactions at the single-molecule level requires tapping into the full spectrum of STM capabilities and the judicious choice of adsorbate–substrate systems for investigation. The STM junction is effectively a nanoreactor in which the metallic tip and the substrate work together to induce chemical transformations of individual molecules adsorbed on the substrate or the tip.

A. Metal carbonyl formation

The manipulation capability of the STM allows the two reactants to be brought close to each other for the reaction to occur. There are two general kinds of manipulation, corresponding to transferring a molecule to the tip and translating a molecule on the surface. Depending on the adsorbate and substrate, one kind of manipulation may be more appropriate than the other and some systems may be difficult to manipulate. It is by trying different conditions (bias voltage, tunneling current, sliding, pulling, pushing, or transferring to the tip) that a manipulation scheme is determined.

The reversible transfer of a molecule between the tip and the substrate is reproducibly achieved for CO on Ag with a polycrystalline W tip. The presence of the CO on the tip is confirmed in three different ways. First, the CO can be transferred back to surface. Second, the imaging resolution is enhanced and new vibrational mode can be excited compared to the bare W tip.[185] Third, CO vibrations can be detected when the CO-terminated tip is positioned above the clean part of the surface. In Fig. 30, a CO molecule is transferred to the tip and the CO-terminated tip is translated and positioned directly over a coadsorbed Fe atom on Ag(110) at 13 K.[186] By applying a current in the reversed direction, the CO is released from the tip and the tunneling current simultaneously stimulated the bonding of the CO to the Fe atom to form iron monocarbonyl (FeCO).[186] This process can be repeated to produce iron dicarbonyl $[Fe(CO)_2]$.

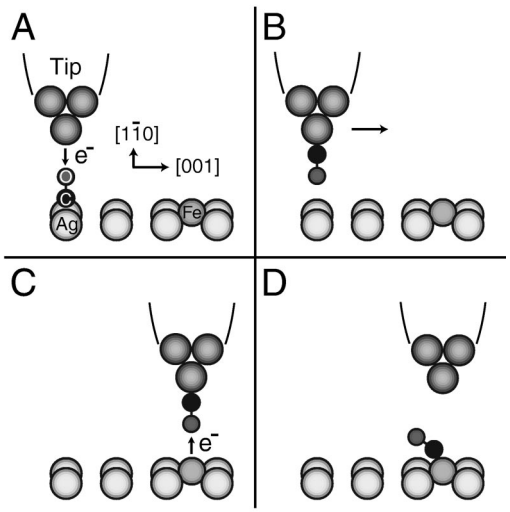

FIG. 30. Schematic diagram showing the different steps in the formation of a single bond with the STM. (A) The tip is positioned over a single CO molecule to induce the detachment of CO from Ag and its bonding to the tip. (B) The tip with the attached single CO molecule is translated (indicated by the arrow) and positioned over an Fe atom. (C) The bias voltage and the flow of electrons are reversed, inducing the transfer of CO from the tip to the Fe. (D) A single Fe–CO bond is formed. [H.J. Lee and W. Ho, Science **286**, 1719 (1999).]

The STM topographic images of the reactants and products on Ag(110) are shown in Fig. 31. The four species are distinguishable from each other and can thus be used for chemical identification. In the case of FeCO, an asymmetric image with a lobe on one side suggests that CO is bonded in a tilted configuration on an Fe atom. Spatially resolved vi-

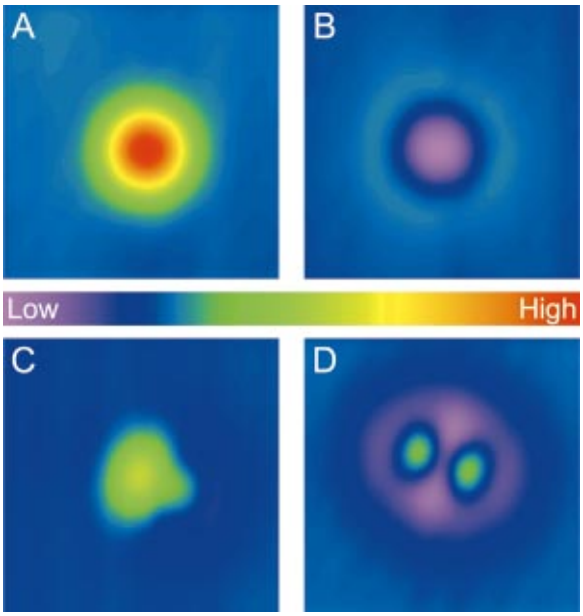

FIG. 31. (Color) 25 Å×25 Å STM topographic images for (A) Fe, (B) CO, (C) Fe(CO), and (D) $Fe(CO)_2$. [H.J. Lee and W. Ho, Science **286**, 1719 (1999).]

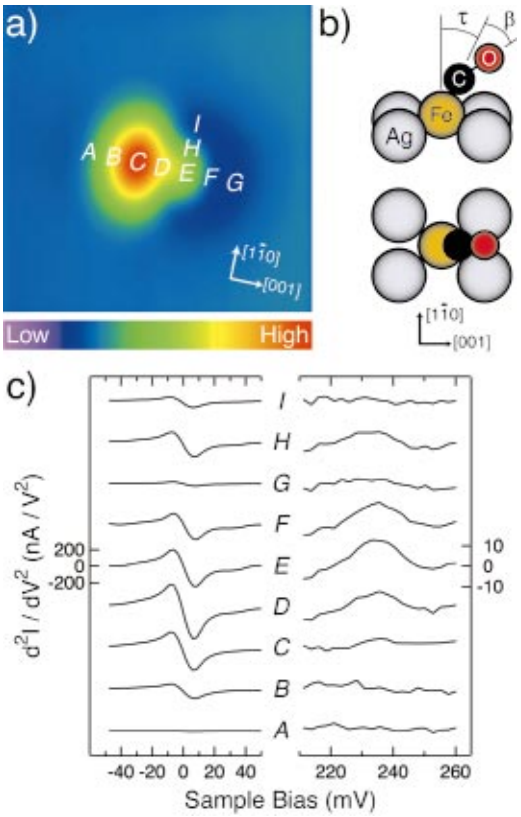

FIG. 32. (Color) (a) 25 Å×25 Å STM topographic image of Fe(CO). Letters A through I denote the tip position for the corresponding vibrational spectra shown in (c). (b) The side and top views of Fe(CO) showing the CO to be tilted by angle τ and bent by an angle β as suggested by the asymmetry in the STM image and the spatial distribution of the vibrational intensity. (c) Spatially resolved, background subtracted single-molecule vibrational spectra of Fe(CO). [H.J. Lee and W. Ho, Phys. Rev. B **61**, R16347 (2000).]

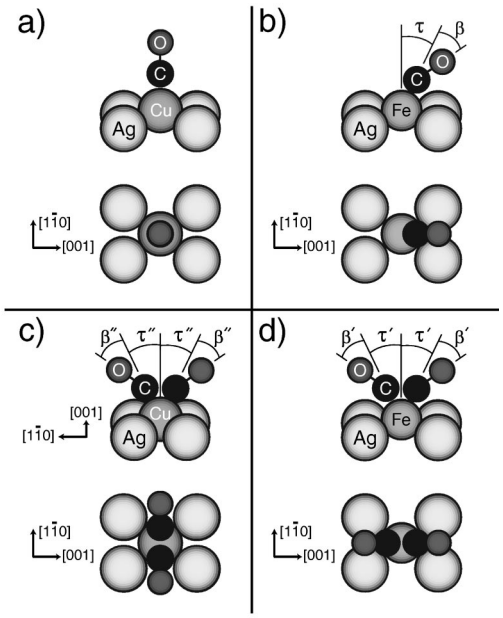

FIG. 33. Schematic diagram of the structures for Cu(CO), Fe(CO), $Cu(CO)_2$, and $Fe(CO)_2$ on Ag(110), synthesized by the manipulation scheme shown in Fig. 30. The orientation of the C–O axis and the plane of the molecule were determined from STM topographic images and spatially resolved STM-IETS on the hindered rotation and the C–O stretch modes.

brational spectroscopy with STM-IETS is uniquely capable of determining the location of the CO molecule in the STM topographic image. Indeed, the lobe in the topographic image is where the CO molecule is since the intensity of the C–O stretch is localized at the lobe, as shown in Fig. 32.

Spatially resolved STM-IETS is capable of structural determination. The contrast in the STM topographic images can sometimes be misleading in deducing the positions of specific bonds. For example, a contrast reversal was observed for acetylene bonded on Cu(001) versus Ni(001).[102] From the analyses of rotational and vibrational motions, the origin of the contrast reversal for acetylene was identified. Similar contrast reversal was also observed between $Fe(CO)_2$ and $Cu(CO)_2$.[187] While the two protrusions in the topographic images of $Fe(CO)_2$ correspond to the two CO ligands, the positions of the two CO ligands in $Cu(CO)_2$ give rise to depressions and are 90° rotated from the orientations of the CO molecules in $Fe(CO)_2$.[187] Furthermore, the CO bond axis is perpendicular to the surface in CuCO, in contrast to the tilted CO bond axis in FeCO.[187] The results from topographic images and spatially resolved spectra by STM-IETS led to the carbonyl structures shown in Fig. 33.

While manipulation of individual CO molecules was used to form iron and copper carbonyls, the CO molecules can preferential bind to individual metal atoms (Pd, Mn) by dosing CO from the gas phase. A search by STM imaging is necessary to locate the carbonyls that have been formed randomly. STM-IETS becomes an important tool for chemical identification of the carbonyls since there is the possibility that impurities contained in the gas may have reacted with the metal atoms. In the case of Pd atoms adsorbed on NiAl(110), the C–O axis is tilted in PdCO and in contrast to $Fe(CO)_2$, the molecular plane of $Pd(CO)_2$ is rotated 90° from that of PdCO.[188] A single Mn atom on NiAl(110) was found to bind up to four CO molecules, with distinct images for MnCO, $Mn(CO)_2$, $Mn(CO)_3$, and $Mn(CO)_4$, showing a protrusion for each CO ligand.[189]

B. Oxidation reaction

The formation of CO_2 by the catalytic oxidation of CO at metal surfaces has been studied extensively by nearly all available surface science techniques. However, the intermediates have not been directly observed and characterized and the microscopic understanding of this reaction is thus incomplete.

In bimolecular surface reactions, two mechanisms have long dominated the discussions. One of the molecules may impinge from the gas phase and react with the second reactant which is adsorbed on the surface, the so-called Eley–Rideal mechanism. The two reactants, however, may both reside on the surface and diffusion brings them together for the reaction through the Langmuir–Hinshelwood mechanism. Conceptually, both these mechanisms are plausible. However, it is not often straightforward to decide unambiguously between these two mechanisms.

The oxidation of CO at the single-molecule level provides definitive understanding into the mechanisms of this

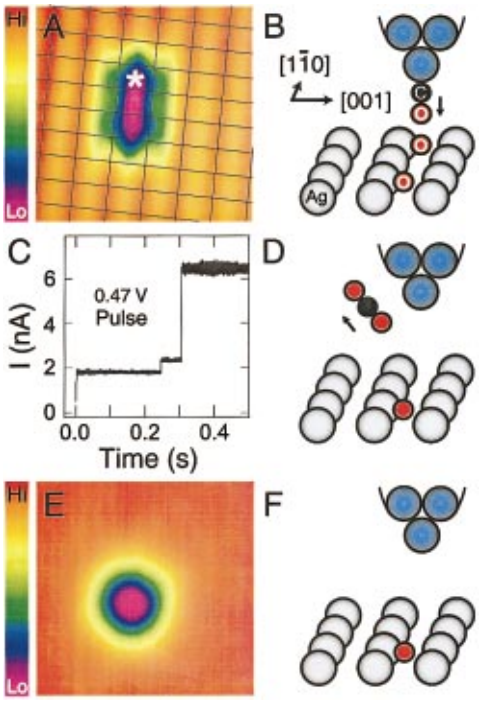

FIG. 34. (Color) Reaction of a CO molecule released from a CO-terminated tip with an O atom adsorbed on the surface. (A) STM topographic image, taken with a CO-terminated tip, of the two O atoms separated by two-lattice spacings (2×2.89 Å) along the [110] direction. Grid lines are drawn through the Ag surface atoms. (C) Tunneling current during a +470 mV sample bias pulse with the CO-terminated tip over one of the two O atoms [denoted by "*" in (A)]. Two current rises at 250 ms and 310 ms indicate the moment of desorption and reaction of CO from the tip and the moment of desorption of CO_2 from the surface. (E) STM topographic image of the same area rescanned after the pulse, showing CO on the tip has reacted away since substrate atoms are no longer resolved. Scan area of (A) and (E) is 25 Å×25 Å. (B), (D), and (F) are the schematic diagrams for (A), (C), and (E), respectively. [J.R. Hahn and W. Ho, Phys. Rev. Lett. **87**, 166102 (2001).]

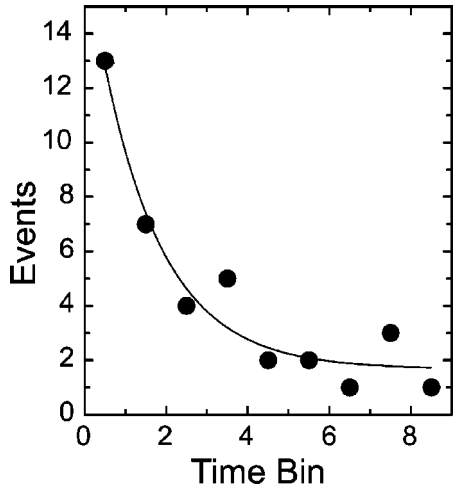

FIG. 35. Distribution of the time interval between the release and reaction of CO from the tip and the desorption of CO_2 from the surface, e.g., 60 ms between 250 ms and 310 ms in Fig. 34 (C). An exponential distribution is obtained. The bin width is 10 ms.

reaction. These results provide a general understanding into some of the key ingredients for the formation of chemical bonds. They offer us a framework for thinking about chemical reactions. The picture that emerges from these studies is especially vivid since the STM provides control and visualization of the oxidation reaction at the single-molecule level.

Similar to the formation of metal carbonyls, a CO molecule is transferred to the tip and is brought into close proximity of a oxygen atom when the CO-terminated tip is positioned directly over the oxygen atom, as shown in Fig. 34. By applying a voltage pulse exceeding the threshold voltage of ~440 mV, CO is released and reacted with the O atom to form CO_2 which desorbs from the surface.[190] The reaction is spatially localized since a nearby oxygen atom, 5.78 Å away (two lattice spacings), is not perturbed.

The time trace of the tunneling current reveals two sudden transitions, at ~0.24 s and ~0.3 s. The time interval between these transitions, ~60 ms, is attributed to the duration between the release of the CO and the desorption of CO_2. The nature of the intermediate step is not apparent but presumably involve interaction between the CO and O. Consistent with the statistics of single-molecule behavior, the time duration of this intermediate step follows an exponential distribution, as illustrated in Fig. 35.

The two reactants, CO and oxygen atom, can be brought close to each other by manipulating the CO molecule on the surface. A schematic diagram illustrating this approach is shown in Fig. 36. A pair of oxygen atoms is produced by dissociating an oxygen molecule with tunneling electrons. The CO molecule is moved toward the pair of oxygen atoms by applying a voltage pulse (~0.25 V) over the CO molecule. In this way, the CO molecule can be positioned at various distances from the oxygen atoms. At the closest separation, the CO is displaced from the top site toward the oxygen atoms. In addition, the C–O axis is tilted with the oxygen end inclined away from the oxygen atoms. It is at this closest distance that a reaction to produce CO_2 can be induced by tunneling electrons.

The combination of imaging, manipulation, spatially resolved STM-IETS, and chemical modification made it pos-

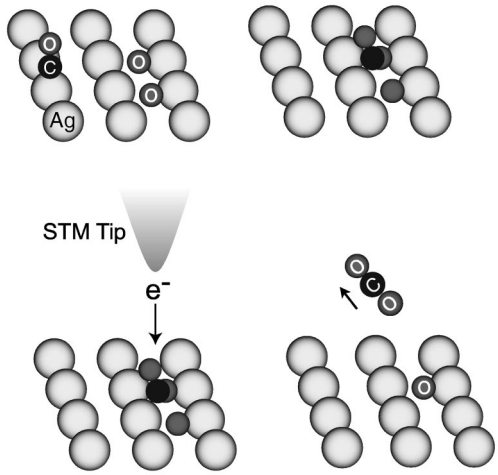

FIG. 36. Schematic diagram illustrating the manipulation of CO toward a pair of oxygen atoms on Ag(110). At the closest separation of the reactants, CO_2 production can be stimulated by tunneling electrons. The CO_2 desorbs from the surface, leaving one oxygen atom behind. A tilted CO structure has been determined for the O–CO–O intermediate complex.

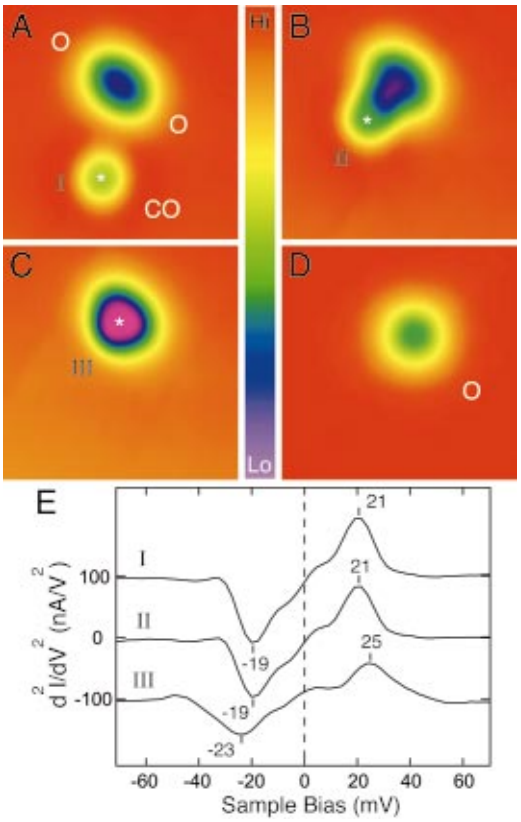

FIG. 37. (Color) STM topographic images obtained with a bare tip, showing the manipulation of a CO molecule toward two O atoms coadsorbed on Ag(110) at 13 K and the corresponding vibrational spectra taken over the CO. (A) A single CO molecule with two O atoms. (B) The CO was moved toward O atoms by applying sample bias pulses (+240 mV) after positioning the tip over it. (C) The CO was moved to the closest distance from the two O atoms to form the O–CO–O complex. (D) An additional voltage pulse applied to the CO side of the complex led to an image of the remaining O atom on the surface. Scan area of (A)–(D) is 29 Å×29 Å. (E) Single-molecule vibrational spectra obtained by STM-IETS for CO at positions marked by *'s in (A)–(C). The line markers indicate the positions of the vibrational features corresponding to the CO hindered rotation. [J.R. Hahn and W. Ho, Phys. Rev. Lett. **87**, 166102 (2001).]

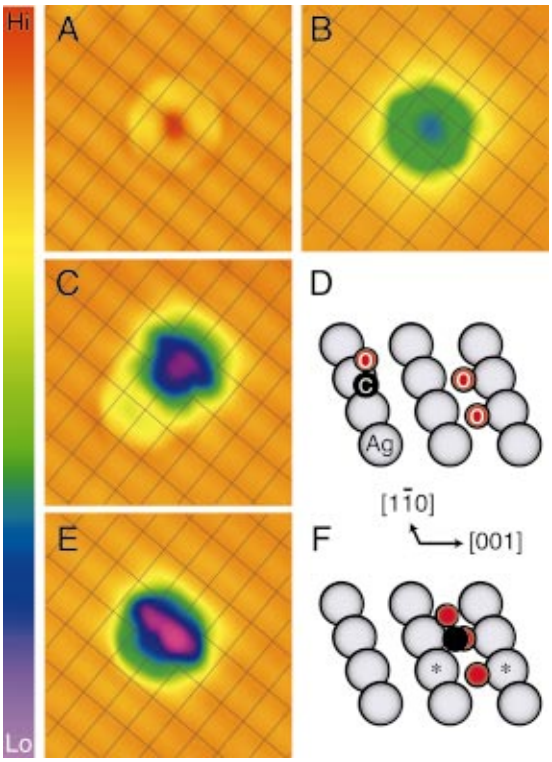

FIG. 38. (Color) STM topographic images obtained with a CO-terminated tip on Ag(110) at 13 K. (A) Isolated CO molecule (on top site adsorption), (B) two oxygen atoms adsorbed on the nearest fourfold hollow sites along the [110] direction. (C) CO and two O atoms separated by 6.1 Å along the [001] direction, and (E) O–CO–O complex. (C) and (E) correspond to Fig. 37(B) and 37(C), respectively. Grid lines are drawn through the Ag surface atoms. Scan area of (A)–(C) and (E) is 25 Å×25 Å. Schematic diagrams for adsorption geometries of (C) and (E) are shown in (D) and (F), respectively; a linear atop and a tilted off-site CO are implicated. [J.R. Hahn and W. Ho, Phys. Rev. Lett. **87**, 166102 (2001).]

sible to capture the reaction intermediate and answer the question of how close the two reactants have to be in order for the reaction to occur. Vibrational spectra were obtained at various separations of the CO from the two oxygen atoms. The hindered rotational mode of CO showed a change only when the CO is at the closest separation from the two oxygen atoms, as shown in Fig. 37. The vibrational energy characterizes the intermediate O–CO–O for this oxidation reaction.

The topographic images in Fig. 37 can be enhanced by imaging with a CO-terminated tip, as shown in Fig. 38.[185] From these enhanced images, the underlying Ag(110) lattice is resolved and the binding sites of CO and the two oxygen atoms can be determined. The manipulated formation of the O–CO–O intermediate is captured frame-by-frame as the CO is moved closer to the two oxygen atoms. The structure of the O–CO–O intermediate is further characterized by the spatial distribution of the hindered rotation, recorded simultaneously with the topographic image. The spatial distribution shows that the intensity of the hindered rotation is shifted away from above a Ag atom toward the two oxygen

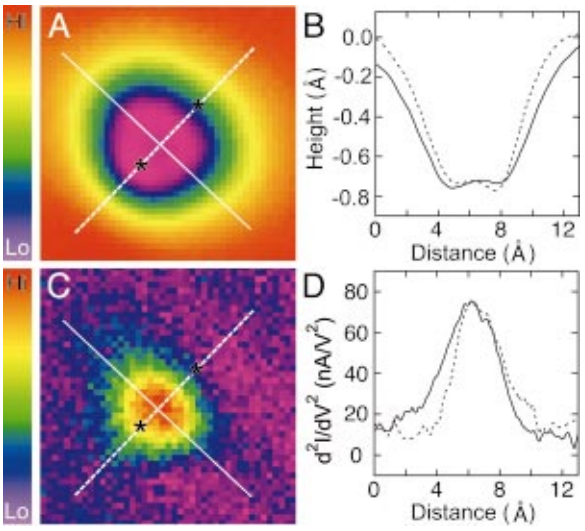

FIG. 39. (Color) Comparison of the topographic image of the O–CO–O complex and the spatial distribution of STM-IETS intensity for the hindered rotation mode of CO on Ag(110) at 13 K. (A) Topographic image taken with a bare tip. (B) Cross sections of (A) taken along the [1$\bar{1}$0] direction (solid line) and the [001] (dashed line) directions. (C) Vibrational microscopy obtained simultaneously with (A) for the hindered rotation of CO. (D) Cross sections of (C) taken along the two directions. The raw data, 14 Å×14 Å, are shown with a resolution of 0.3 Å per pixel. Two Ag atoms shown in Fig. 38(F) are marked by "*" in both topographic and vibrational images. [J.R. Hahn and W. Ho, Phys. Rev. Lett. **87**, 166102 (2001).]

atoms, as revealed in Fig. 39. When the CO is further away from the two oxygen atoms, it is adsorbed on top of a Ag atom and the spatial distribution of the hindered rotation is centered on that Ag atom.

C. Hydrogen transfer reaction

The transfer of a hydrogen atom between two species constitutes an important class of bimolecular reactions. The STM was used to move a H_2S molecule next to a dicarbon species (CC) on Cu(001) 9 K.[191,192] Even at this low temperature, the hydrogen is readily transferred as soon as the two reactants are next to each other to form HS and CCH on the surface. The two products remain close to each other but can be moved apart to reveal more clearly their identities. The manipulation of H_2S toward the CC and the formation of the products are shown in Fig. 40. The characteristic rotational motion of the ethynyl product (CCH) is readily observed, providing a quick fingerprint of the molecule.

Transfer of the hydrogen atom to CC also occurs readily with H_2O.[192] In contrast to H_2S which is stationary but moves by tunneling electrons, the H_2O diffuses readily on the Cu(001) surface at 9 K. The water molecule can be trapped by the ethynyl, without transferring a hydrogen atom, or by an impurity or at a step. When the water molecule encounters a dicarbon species, a single hydrogen atom is transferred from the H_2O to the CC, forming OH and CCH on the surface. The two products are close to each other such that their images overlap. The OH species is bonded to the surface more strongly than H_2O, enabling a stationary image to be obtained. The two products are separated and their images become resolved after manipulation with tunneling electrons.

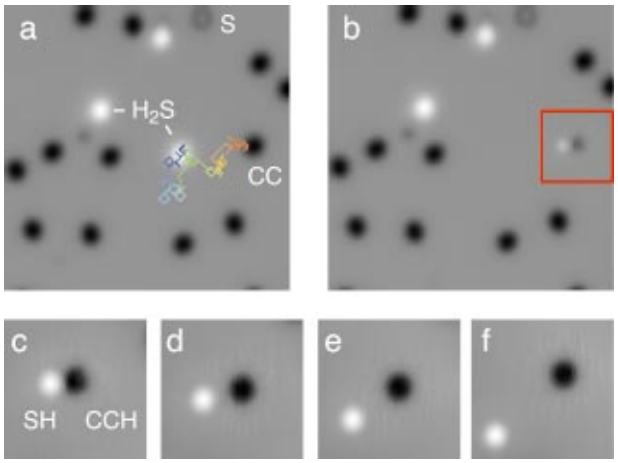

FIG. 40. (Color) Single H atom transfer from H_2S to CC on Cu(001) at 9 K. (a) 100 Å×100 Å STM topographic image of H_2S and CC. By exciting the H_2S with tunneling electrons at 0.1 nA and 250 mV sample bias, the H_2S hop between lattice sites in a random manner. The path of the tip following the adsorbate motion is indicated by the colored line. (b) STM image taken after the induced diffusion. The H_2S has reacted with CC. The product SH is less bright than the reactant H_2S. (c) 30 Å×30 Å image of the area in the red box of panel (b) showing the newly formed SH and CCH reaction products. (d)–(f) The SH was separated from the CCH by induced diffusion to show the products more clearly. The CCH rotates rapidly under the imaging conditions. This rotation is responsible for the streaky halo around the depression. [L.J. Lauhon and W. Ho, J. Phys. Chem. B **105**, 3987 (2001).]

The formation of metal–carbon, carbon–oxygen, and carbon–hydrogen bonds have been demonstrated with the STM. The simple molecules chosen to demonstrate the feasibility of STM induced bond formation enable detailed information to be obtained. The formation of carbon–carbon bond has been reported for the production of biphenyl from two iodobenzene molecules at the step edge of a Cu(111) surface at 20 K.[193] Evidence for the formation of the carbon–carbon bond in the biphenyl was based on the observation that the image of the newly formed species moved as an entity when manipulated by the STM in the pulling mode. Spectroscopic data would further support the formation of the carbon–carbon bond since the two phenyl rings may interact indirectly through the substrate. Such indirect interactions are responsible for the observation of the reversible rotation of antimony dimers on Si(100) even though there is no direct bonding between the two antimony atoms.[137]

X. CONCLUDING REMARKS AND FUTURE PROSPECTS

Inelastic electron tunneling spectroscopy with the STM (STM-IETS) allows us to reach the limit of sensitivity of vibrational spectroscopy, that of a single bond. While this represents an approximately nine orders of magnitude increase in sensitivity, an additional uniqueness of STM-IETS lies in the scanning capability of the microscope for providing the spatial distribution of the vibrational intensity with sub-angstrom resolution. By combining single-molecule vibrational spectroscopy and microscopy with the unmatched imaging, manipulation, and chemical modification capabilities of the STM, chemistry can be probed at the spatial limit of single atoms and single bonds. Direct visualization of the nature of the chemical bonds and their transformations at the single-molecule level not only provides convincing evidences but also fundamental understandings of chemical processes.

The value of direct visualization cannot be overstated. Our sense of vision has played an important role in our understanding of the world around us. It is not surprising that the ability to see things often dispels much of our doubts and removes uncertainties and ambiguities surrounding the system under investigation. In chemistry, the basic building blocks are the electrons, protons, and neutrons, and the fundamental force is the Coulomb force. Chemistry is concerned with how the electrons couple to the nuclear motions and how atoms and molecules interact with each other to break and form bonds. Thus the ability to see atoms and molecules and directly visualize the vibrational, rotational, and translational motions, the energy transfer, conformation change, the electrical conductivity, the dissociation of single bonds, and the formation of individual bonds, all at the single-molecule level, provides us with a fresh view and in many instances new insights into chemistry. STM provides us with direct visualization of quantum mechanics.

The most detailed information enabled by the STM has come from studying atoms and small molecules where the structure is more readily determined. Application of the STM to the study of larger molecules is certainly possible. However, results pertaining to the properties of single bonds are

relevant to understanding the behavior of large molecules since many aspects of chemistry are local in nature and involve a few bonds in specific locations of the molecule.

The range of application of the STM is broadening in time. The study of single-molecule chemistry is expected to remain a fertile area of research for many years to come. The whole field of surface science can be revisited by the STM. In addition to the many opportunities for experimental investigation (some of the most exciting ones certainly have not been identified), there is a great need for theoretical work. The coupling of electrons to nuclear motions includes problems dealing with the mechanistic understanding of STM-IETS and chemistry induced by tunneling electrons. Many of these problems involve the excited states (or the empty states) which present particular challenges to theoretical analysis.

The measurement of the electrical conductivity of single molecules provides a new way of probing their properties. While measurement of the conductivity through the tunneling gap is valuable, it is also desirable to make direct contact, i.e., bonding, between the molecule and the tip with the other end of the molecule bonded to the substrate. The molecule can even be put under stress by stretching it while measuring the conductivity through it. Vibrational spectroscopy is entirely feasible in such direct contact configuration.

One of the fundamental problems in solid state physics concerns the transition from a single atom to the bulk solid. The STM can be used to manipulate individual atoms to construct increasingly large systems in one, two, and even three dimensions one atom at a time.[194] Spatially resolved spectroscopy can be used effectively to monitor the evolution of the electronic structure as the system evolves from a single atom to a bulk solid. The bonding of molecules to such artificial solids is expected to reveal unusual properties and chemistry. Since these artificial solids are built atom by atom, materials with novel composition, stoichiometry, structure, and properties are envisioned.

The combination of optics with the STM leads to a new regime of experimental investigation of single molecules. Light emission from single molecules stimulated by tunneling electrons is expected to provide new insights into the electronic and vibrational structure and energy transfer pathways in a molecule.[81] These experiments provide an opportunity to correlate molecular conformations with light emission efficiency and spectral distribution.

An area in nanoscience that is attracting a great deal of attention lies in the use of the STM to probe electron spin properties in nanoscale systems.[195] Spectroscopy on the spin excitations of single atoms and molecules requires STMs operating at low temperatures (<1 K) and high magnetic fields (>5 Tesla). These experiments will provide a new way to probe the magnetic properties of single molecules.

The excitement of single-molecule chemistry is expected to continue, with many new discoveries which are not anticipated at the present time. The extreme spatial confinement of energetic electrons in the STM tunnel junction continues to provide an effective and unique approach to probe the inner workings of single molecules and their interactions with the surroundings.

ACKNOWLEDGMENTS

It is a great pleasure and privilege for me to have worked with the gifted and dedicated graduate students and postdoctoral associates on the exploration of single-molecule chemistry with the scanning tunneling microscopes: Xi Chen, Jennifer Gaudioso, Jae Ryang Hahn, Lincoln Lauhon, Hyojune Lee, George Nazin, Niklas Nilius, Xiaohui Qiu, Mohammad Rezaei, Barry Stipe, and Mitch Wallis. In addition, we have benefited greatly from discussions and collaborations with Shiwu Gao, Nicolas Lorente, and Mats Persson. The selected work which have been presented in this manuscript were carried out over the last 5 years. We are grateful for the support provided by the National Science Foundation and the Chemical Science, Geo and Bioscience Division, Office of Science, U.S. Department of Energy.

[1] H. Noji, R. Yasuda, M. Yoshida, and K. Kinosita, Jr., Nature (London) **386**, 299 (1997).
[2] W.E. Moerner and L. Kador, Phys. Rev. Lett. **62**, 2535 (1989).
[3] M. Orrit and J. Bernard, Phys. Rev. Lett. **65**, 2716 (1990).
[4] E. Betzig and R.J. Chichester, Science **262**, 1422 (1993).
[5] J.K. Trautman and J.J. Macklin, Chem. Phys. **205**, 221 (1996).
[6] E.J. Sánchez, L. Novotny, and X.S. Xie, Phys. Rev. Lett. **82**, 4014 (1999).
[7] S. Nie and S.R. Emory, Science **275**, 1102 (1997).
[8] W.E. Moerner, Science **265**, 46 (1994).
[9] W.P. Ambrose and W.E. Moerner, Nature (London) **349**, 225 (1991).
[10] J. Bernard, L. Fleury, H. Talon, and M. Orrit, J. Chem. Phys. **98**, 850 (1993).
[11] Th. Basché, W.E. Moerner, M. Orrit, and H. Talon, Phys. Rev. Lett. **69**, 1516 (1992).
[12] J. Köhler, J.A.J.M. Disselhorst, M.C.J.M. Donckers, E.J.J. Groenen, J. Schmidt, and W.E. Moerner, Nature (London) **363**, 242 (1993).
[13] J. Wrachtrup, C. von Borczyskowski, J. Bernard, M. Orrit, and R. Brown, Nature (London) **363**, 244 (1993).
[14] W.P. Ambrose, P.M. Goodwin, J.C. Martin, and R.A. Keller, Science **265**, 364 (1994).
[15] X.S. Xie and R.C. Dunn, Science **265**, 361 (1994).
[16] S. Nie, D.T. Chiu, and R.N. Zare, Science **266**, 1018 (1994).
[17] W.P. Ambrose, P.M. Goodwin, J.C. Martin, and R.A. Keller, Phys. Rev. Lett. **72**, 160 (1994).
[18] J.K. Trautman, J.J. Macklin, L.E. Brus, and E. Betzig, Nature (London) **369**, 40 (1994).
[19] S. Weiss, Science **283**, 1676 (1999); A.D. Mehta, M. Rief, J.A. Spudich, D.A. Smith, and R.M. Simmons, *ibid.*, **283**, 1689.
[20] T. Ha, Th. Enderle, D.F. Ogletree, D.S. Chemla, P.R. Selvin, and S. Weiss, Proc. Natl. Acad. Sci. U.S.A. **93**, 6264 (1996).
[21] D.A. Vanden Bout, W.-T. Yip, D. Hu, D.-K. Fu, T.M. Swager, and P.F. Barbara, Science **277**, 1074 (1997).
[22] R.M. Dickson, A.B. Cubitt, R.Y. Tsien, and W.E. Moerner, Nature (London) **388**, 355 (1997).
[23] H.P. Lu, L. Xun, and X.S. Xie, Science **282**, 1877 (1998).
[24] M. Bruchez, Jr., M. Moronne, P. Gin, S. Weiss, and A.P. Alivisatos, Science **281**, 2013 (1998).
[25] W.C.W. Chan and S. Nie, Science **281**, 2016 (1998).
[26] A. Ashkin, J.M. Dziedzic, J.E. Bjorkholm, and S. Chu, Opt. Lett. **11**, 288 (1986).
[27] S. Chu, Science **253**, 861 (1991).
[28] H. Ying, M.D. Wang, K. Svoboda, R. Landick, S.M. Block, and J. Gelles, Science **270**, 1653 (1995).
[29] J.T. Finer, R.M. Simmons, and J.A. Spudich, Nature (London) **368**, 113 (1994).
[30] A. Ishijima, H. Kojima, T. Funatsu, M. Tokunaga, H. Higuchi, H. Tanaka, and T. Yanagida, Cell **92**, 161 (1998).
[31] H. Higuchi, E. Muto, Y. Inoue, and T. Yanagida, Proc. Natl. Acad. Sci. U.S.A. **94**, 4395 (1997).
[32] M.J. Schnitzer and S.M. Block, Nature (London) **388**, 386 (1997).
[33] W. Hua, E.C. Young, M.L. Fleming, and J. Gelles, Nature (London) **388**, 390 (1997).
[34] C. Shingyoji, H. Higuchi, M. Yoshimura, E. Katayama, and T. Yanagida, Nature (London) **393**, 711 (1998).

[35] M.S. Kellermayer, S.B. Smith, H.L. Granzier, and C. Bustamante, Science **276**, 1112 (1997).
[36] L. Tskhovrebova, J. Trinick, J.A. Sleep, and R.M. Simmons, Nature (London) **387**, 308 (1997).
[37] S.B. Smith, L. Finzi, and C. Bustamante, Science **258**, 1122 (1992).
[38] T.R. Strick, J.-F. Allemand, D. Bensimon, A. Bensimon, and V. Croquette, Science **271**, 1835 (1996).
[39] A. Ashkin and J.M. Dziedzic, Proc. Natl. Acad. Sci. U.S.A. **86**, 7914 (1989).
[40] L.A. Bumm, J.J. Arnold, M.T. Cygan, T.D. Dunbar, T.P. Burgin, L. Jones II, D.L. Allara, J.M. Tour, and P.S. Weiss, Science **271**, 1705 (1996).
[41] M.A. Reed, C. Zhou, C.J. Muller, T.P. Burgin, and J.M. Tour, Science **278**, 252 (1997).
[42] J. Park, A.N. Pasupathy, J.I. Goldsmith, C. Chang, Y. Yaish, J.R. Petta, M. Rinkoski, J.P. Sethna, H.D. Abruña, P.L. McEuen, and D.C. Ralph, Nature (London) **417**, 722 (2002).
[43] W. Liang, M.P. Shores, M. Bockrath, J.R. Long, and H. Park, Nature (London) **417**, 725 (2002).
[44] J.W.G. Wildoer, L.C. Venema, A.G. Rinzler, R.E. Smalley, and C. Dekker, Nature (London) **391**, 59 (1998).
[45] T.W. Odom, J.-L. Huang, P. Kim, and C.M. Lieber, Nature (London) **391**, 62 (1998).
[46] H. Dai, E.W. Wong, and C.M. Lieber, Science **272**, 523 (1996).
[47] S.J. Tans, M.H. Devoret, H. Dai, A. Thess, R.E. Smalley, L.J. Georliga, and C. Dekker, Nature (London) **386**, 474 (1997).
[48] A.Yu. Kasumov, R. Deblock, M. Kociak, B. Reulet, H. Bouchiat, I.I. Khodos, Yu.B. Gorbatov, V.T. Volkov, C. Journet, and M. Burghard, Science **284**, 1508 (1999).
[49] A. Bachtold, C. Strunk, J.-P. Salvetat, J.-M. Bonard, L. Forro, T. Nussbaumer, and C. Schonenberger, Nature (London) **397**, 673 (1999).
[50] K. Tsukagoshi, B.W. Alphenaar, and H. Ago, Nature (London) **401**, 572 (1999).
[51] Z. Yao, H.W.Ch. Postma, L. Balents, and C. Dekker, Nature (London) **402**, 273 (1999).
[52] M.S. Fuhrer, J. Nygard, L. Shih, M. Forero, Y.-G. Yoon, M.S.C. Mazzoni, H.J. Choi, J. Ihm, S.G. Louie, A. Zettl, and P.L. McEuen, Science **288**, 494 (2000).
[53] S.J. Wind, J. Appenzeller, R. Martel, V. Derycke, and Ph. Avouris, Appl. Phys. Lett. **80**, 3817 (2002).
[54] G. Binnig, Ch. Gerber, E. Stoll, T.R. Albrecht, and C.F. Quate, Europhys. Lett. **3**, 1281 (1987).
[55] P.K. Hansma, V.B. Elings, O. Marti, and C.E. Bracker, Science **242**, 209 (1988).
[56] B. Drake, C.B. Prater, A.L. Weisenhorn, S.A.C. Gould, T.R. Albrecht, C.F. Quate, D.S. Cannell, H.G. Hansma, and P.K. Hansma, Science **243**, 1586 (1989).
[57] M. Radmacher, R.W. Tillmann, M. Fritz, and H.E. Gaub, Science **257**, 1900 (1992).
[58] W.A. Rees, R.W. Keller, J.P. Vesenka, G. Yang, and C. Bustamante, Science **260**, 1646 (1993).
[59] M. Radmacher, M. Fritz, H.G. Hansma, and P.K. Hansma, Science **265**, 1577 (1994).
[60] C.D. Frisbie, L.F. Rozsnyai, A. Noy, M.S. Wrighton, and C.M. Lieber, Science **265**, 2071 (1994).
[61] H. Takano, J.R. Kenseth, S.S. Wong, J.C. O'Brien, and M.D. Porter, Chem. Rev. **99**, 2845 (1999).
[62] R. McKendry, M.-E. Theoclitou, T. Rayment, and C. Abell, Nature (London) **391**, 566 (1998).
[63] S.S. Wong, E. Joselevich, A.T. Woolley, C.L. Cheung, and C.M. Lieber, Nature (London) **394**, 52 (1998).
[64] C.L. Cheung, J.H. Hafner, and C.M. Lieber, Proc. Natl. Acad. Sci. U.S.A. **97**, 3809 (2000).
[65] K. Wago, D. Botkin, C.S. Yannoni, and D. Rugar, Phys. Rev. B **57**, 1108 (1998).
[66] M. Rief, M. Gautel, F. Oesterhelt, J.M. Fernandez, and H.E. Gaub, Science **276**, 1109 (1997).
[67] A.F. Oberhauser, P.E. Marszalek, H.P. Erickson, and J.M. Fernandez, Nature (London) **393**, 181 (1998).
[68] M. Rief, F. Oesterhelt, B. Heymann, and H.E. Gaub, Science **275**, 1295 (1997).
[69] E.L. Florin, V.T. Moy, and H.E. Gaub, Science **264**, 415 (1994).
[70] J. Fritz, A.G. Katopodis, F. Kolbinger, and D. Anselmetti, Proc. Natl. Acad. Sci. U.S.A. **95**, 12283 (1998).
[71] R. Ros, F. Schwesinger, D. Anselmetti, M. Kubon, R. Schafer, A. Pluckthun, and L. Tiefenauer, Proc. Natl. Acad. Sci. U.S.A. **95**, 7402 (1998).
[72] O.H. Willemsen, M.M.E. Snel, K.O. van der Werf, B.G. de Grooth, J. Greve, P. Hinterdorfer, H.J. Gruber, H. Schindler, Y. van Kooyk, and C.G. Figdor, Biophys. J. **75**, 2220 (1998).
[73] P. Sautet, Chem. Rev. **97**, 1097 (1997).
[74] Y. Kuk, D.K. Kim, Y.D. Suh, K.H. Park, H.P. Noh, S.J. Oh, and S.K. Kim, Phys. Rev. Lett. **70**, 1948 (1993).
[75] C. Rogero, J.I. Pascual, J. Gómez-Herrero, and A.M. Baró, J. Chem. Phys. **116**, 832 (2002).
[76] X.H. Qiu, G.V. Nazin, and W. Ho (unpublished).
[77] B.C. Stipe, M.A. Rezaei, and W. Ho, Science **280**, 1732 (1998).
[78] R. Berndt, R. Gaisch, J.K. Gimzewski, B. Reihl, R.R. Schlittler, W.D. Schneider, and M. Tschudy, Science **262**, 1425 (1993).
[79] K. Sakamoto, K. Meguro, R. Arafune, M. Satoh, Y. Uehara, and S. Ushioda, Surf. Sci. **502**, 149 (2002).
[80] G. Hoffmann, L. Libioulle, and R. Bernt, Phys. Rev. B **65**, 212107 (2002).
[81] X.H. Qiu, G.V. Nazin, and W. Ho (unpublished).
[82] P. Tchénio, A.B. Myers, and W.E. Moerner, J. Phys. Chem. **97**, 2491 (1993).
[83] K. Kneipp, Y. Wang, H. Kneipp, L.T. Perelman, I. Itzkan, R.R. Dasari, and M.S. Feld, Phys. Rev. Lett. **78**, 1667 (1997).
[84] S. Nie and S.R. Emory, Science **275**, 1102 (1997).
[85] R.M. Stöckle, Y.D. Suh, V. Deckert, and R. Zenobi, Chem. Phys. Lett. **318**, 131 (2000).
[86] M.S. Anderson, Appl. Phys. Lett. **76**, 3130 (2000).
[87] A.B. Myers, P. Tchénio, M.Z. Zgierski, and W.E. Moerner, J. Phys. Chem. **98**, 10377 (1994).
[88] B. Lounis, F. Jelezko, and M. Orrit, Phys. Rev. Lett. **78**, 3673 (1997).
[89] K. Kneipp, H. Kneipp, V.B. Kartha, R. Manoharan, G. Deinum, I. Itzkan, R.R. Dasari, and M.S. Feld, Phys. Rev. E **57**, R6281 (1998).
[90] K. Kneipp, H. Kneipp, I. Itzkan, R.R. Dasari, and M.S. Feld, Chem. Phys. **247**, 155 (1999).
[91] S.R. Emory and S. Nie, J. Phys. Chem. B **102**, 493 (1998).
[92] S.R. Emory, W.E. Haskins, and S. Nie, J. Am. Chem. Soc. **120**, 8009 (1998).
[93] K. Kneipp, H. Kneipp, G. Deinum, I. Itzkan, R.R. Dasari, and M.S. Feld, Appl. Spectrosc. **52**, 175 (1998).
[94] A.M. Michaels, M. Nirmal, and L.E. Brus, J. Am. Chem. Soc. **121**, 9932 (1999).
[95] J.T. Krug II, G.D. Wang, S.R. Emory, and S. Nie, J. Am. Chem. Soc. **121**, 9208 (1999).
[96] H. Xu, E.J. Bjerneld, M. Kåll, and L. Borjesson, Phys. Rev. Lett. **83**, 4357 (1999).
[97] K. Kneipp, H. Kneipp, I. Itzkan, R.R. Dasari, and M.S. Feld, Chem. Rev. **99**, 2957 (1999).
[98] T. Xiao, Q. Ye, and L. Sun, J. Phys. Chem. B **101**, 632 (1997).
[99] H. Xu, J. Aizpurua, M. Kåll, and P. Apell, Phys. Rev. E **62**, 4318 (2000).
[100] K. Kneipp, Spectrochim. Acta, Part A **50**, 1023 (1994).
[101] A. Zumbusch, G.R. Holtom, and X.S. Xie, Phys. Rev. Lett. **82**, 4142 (1999).
[102] B.C. Stipe, M.A. Rezaei, and W. Ho, Phys. Rev. Lett. **82**, 1724 (1999).
[103] R.C. Jaklevic and J. Lambe, Phys. Rev. Lett. **17**, 1139 (1966).
[104] B.C. Stipe, M.A. Rezaei, and W. Ho, Rev. Sci. Instrum. **70**, 137 (1999).
[105] L.J. Lauhon and W. Ho, Rev. Sci. Instrum. **72**, 216 (2001).
[106] B.C. Stipe, Curr. Opin. Solid State Mater. Sci. **4**, 421 (1999).
[107] N. Mingo and K. Makoshi, Phys. Rev. Lett. **84**, 3694 (2000).
[108] N. Lorente and M. Persson, Phys. Rev. Lett. **85**, 2997 (2000).
[109] N. Lorente, M. Persson, L.J. Lauhon, and W. Ho, Phys. Rev. Lett. **86**, 2593 (2001).
[110] N.W. Ashcroft and N.D. Mermin, *Solid State Physics* (Holt, Rinehart and Winston, New York, 1976).
[111] R.L. Dennis and M.B. Webb, J. Vac. Sci. Technol. **10**, 192 (1973).
[112] J.R. Hahn, H.J. Lee, and W. Ho, Phys. Rev. Lett. **85**, 1914 (2000).
[113] J. Gaudioso, L.J. Lauhon, and W. Ho, Phys. Rev. Lett. **85**, 1918 (2000).
[114] J. Gaudioso and W. Ho, Angew. Chem. Int. Ed. Engl. **40**, 4080 (2001).
[115] L.J. Lauhon and W. Ho, J. Phys. Chem. A **104**, 2463 (2000).
[116] *Tunneling Spectroscopy*, edited by P.K. Hansma (Plenum, New York, 1982).
[117] L.J. Lauhon and W. Ho, Phys. Rev. Lett. **84**, 1527 (2000).
[118] J. Gaudioso and W. Ho, J. Am. Chem. Soc. **123**, 10095 (2001).
[119] T.M. Wallis, X. Chen, and W. Ho, J. Chem. Phys. **113**, 4837 (2000).
[120] J. Gaudioso, H.J. Lee, and W. Ho, J. Am. Chem. Soc. **121**, 8479 (1999).
[121] N. Liu, N. Pradhan, J. Gaudioso, and W. Ho (unpublished results).

[122] J.R. Hahn and W. Ho (unpublished results).
[123] L.J. Lauhon and W. Ho, Phys. Rev. B **60**, R8525 (1999).
[124] L.J. Lauhon and W. Ho, Phys. Rev. Lett. **85**, 4566 (2000).
[125] J.I. Pascual and H.-P. Rust (unpublished results and private communications).
[126] J.I. Pascual, J. Gómez-Herrero, D. Sánchez-Portal, and H.-P. Rust (to be published).
[127] J.I. Pascual, J.J. Jackiw, Z. Song, P.S. Weiss, H. Conrad, and H.-P. Rust, Phys. Rev. Lett. **86**, 1050 (2001).
[128] F. Moresco, G. Meyer, and K.H. Rieder, Mod. Phys. Lett. B **13**, 709 (1999).
[129] C.P. Lutz and D.M. Eigler (unpublished results and private communications).
[130] Y. Kim, T. Komeda, and M. Kawai, Phys. Rev. Lett. **89**, 126104 (2002).
[131] *Vibrational Spectroscopy of Molecules on Surfaces*, edited by J.T. Yates, Jr. and T.E. Madey (Plenum, New York, 1987).
[132] Ph. Avouris, D. Schmeisser, and J.E. Demuth, Phys. Rev. Lett. **48**, 199 (1982).
[133] S. Andersson and J. Harris, Phys. Rev. Lett. **48**, 545 (1982).
[134] R.E. Palmer and R.F. Willis, Surf. Sci. **179**, L1 (1987).
[135] K. Svensson, L. Bengtsson, J. Bellman, M. Hassel, M. Persson, and S. Andersson, Phys. Rev. Lett. **83**, 124 (1999).
[136] B.C. Stipe, M.A. Rezaei, and W. Ho, Science **279**, 1907 (1998).
[137] Y.W. Mo, Science **261**, 886 (1993).
[138] B.S. Swartzentruber, A.P. Smith, and H. Jonsson, Phys. Rev. Lett. **77**, 2518 (1996).
[139] J.C. Dunphy, M. Rose, S. Behler, D.F. Ogletree, M. Salmeron, and P. Sautet, Phys. Rev. B **57**, R12705 (1998).
[140] J.K. Gimzewski, C. Joachim, R.R. Schlittler, V. Langlais, H. Tang, and I. Johannsen, Science **281**, 531 (1998).
[141] D. Teillet-Billy, J.P. Gauyacq, and M. Persson, Phys. Rev. B **62**, R13306 (2000).
[142] F.F. Crim, J. Phys. Chem. **100**, 12725 (1996).
[143] E.W.-G. Diau, J.L. Herek, Z.H. Kim, and A.H. Zewail, Science **279**, 847 (1998).
[144] T.J. Chuang, H. Seki, and I. Hussla, Surf. Sci. **158**, 525 (1985).
[145] W. Ho, J. Phys. Chem. **100**, 13050 (1996).
[146] A. Laubereau and W. Kaiser, Rev. Mod. Phys. **50**, 607 (1978).
[147] F. Legay, in *Chemical and Biological Applications of Lasers*, edited by C.B. Moore (Academic, New York, 1977), p. 43.
[148] K.F. Freed and H. Metiu, Chem. Phys. Lett. **48**, 262 (1977).
[149] H. Dubost, Chem. Phys. **12**, 139 (1976).
[150] A.L. Harris, L. Rothberg, L.H. Dubois, N.J. Levinos, and L. Dhar, Phys. Rev. Lett. **64**, 2086 (1990).
[151] P. Guyot-Sionnest, P. Dumas, Y.J. Chabal, and G.S. Higashi, Phys. Rev. Lett. **64**, 2156 (1990).
[152] B.C. Stipe, M.A. Rezaei, and W. Ho, Phys. Rev. Lett. **81**, 1263 (1998).
[153] T.T. Tsong, Surf. Sci. **299/300**, 153 (1993).
[154] R.D. Vale, T. Funatsu, D.W. Pierce, L. Romberg, Y. Harada, and T. Yanagida, Nature (London) **380**, 451 (1996).
[155] Th. Schmidt, G.J. Schutz, W. Baumgartner, H.J. Gruber, and H. Schindler, J. Phys. Chem. **99**, 17662 (1995).
[156] R.M. Dickson, D.J. Norris, Y.-L. Tzeng, and W.E. Moerner, Science **274**, 966 (1996).
[157] L.J. Lauhon and W. Ho, J. Chem. Phys. **111**, 5633 (1999).
[158] L.J. Lauhon and W. Ho, Surf. Sci. **451**, 219 (2000).
[159] B.S. Swartzentruber, Phys. Rev. Lett. **76**, 459 (1996).
[160] R. DiFoggio and R. Gomer, Phys. Rev. B **25**, 3490 (1982).
[161] R. Gomer, Rep. Prog. Phys. **53**, 971 (1990).
[162] T.-S. Lin and R. Gomer, Surf. Sci. **255**, 41 (1991).
[163] E.A. Daniels and R. Gomer, Surf. Sci. **336**, 245 (1995).
[164] A.P. Graham, A. Menzel, and J.P. Toennies, J. Chem. Phys. **111**, 1676 (1999).
[165] X.D. Zhu, T. Rasing, and Y.R. Shen, Phys. Rev. Lett. **61**, 2883 (1988).
[166] X.D. Zhu, Mod. Phys. Lett. B **6**, 1217 (1992).
[167] G.X. Cao, E. Nabighian, and X.D. Zhu, Phys. Rev. Lett. **79**, 3696 (1997).
[168] T.R. Mattsson, U. Engberg, and G. Wahnström, Phys. Rev. Lett. **71**, 2615 (1993).
[169] T.R. Mattsson and G. Wahnström, Phys. Rev. B **56**, 14944 (1997).
[170] L.Y. Chen and S.C. Ying, Phys. Rev. Lett. **73**, 700 (1994).
[171] R. Baer, Y. Zeiri, and R. Kosloff, Surf. Sci. **411**, L783 (1998).
[172] V. Pouthier and J.C. Light, J. Chem. Phys. **113**, 1204 (2000).
[173] L.J. Lauhon and W. Ho, Phys. Rev. Lett. **89**, 079901 (2002). An error of a factor of 2 was discovered for the calculation of the mean-square value of the distance traveled in time t. The corrected version of Fig. 2 in Ref. 124 is shown in Fig. 17 of the present paper.
[174] E. Hill, B. Freelon, and E. Ganz, Phys. Rev. B **60**, 15896 (1999).
[175] M. Dürr, A. Biedermann, Z. Hu, U. Höfer, and T.F. Heinz, Science **296**, 1838 (2002).
[176] J. Kua, L.J. Lauhon, W. Ho, and W.A. Goddard III, J. Chem. Phys. **115**, 5620 (2001).
[177] J. Völkl and G. Alefeld, in *Hydrogen in Metals, I*, edited by G. Alefeld and J. Völkl (Springer-Verlag, New York, 1978), Chap. 12.
[178] E.B. Karlsson, *Solid State Phenomena As Seen by Muons, Protons, and Excited Nuclei* (Oxford University Press, New York, 1995).
[179] V.G. Storchak and N.V. Prokof'ev, Rev. Mod. Phys. **70**, 929 (1998).
[180] T. Komeda, Y. Kim, M. Kawai, B.N.J. Persson, and H. Ueba, Science **295**, 2055 (2002).
[181] B.C. Stipe, M.A. Rezaei, W. Ho, S. Gao, M. Persson, and B.I. Lundqvist, Phys. Rev. Lett. **78**, 4410 (1997).
[182] B.C. Stipe, M.A. Rezaei, and W. Ho, J. Chem. Phys. **107**, 6443 (1997).
[183] W. Ho, J. Phys. Chem. **100**, 13050 (1996).
[184] J.R. Hahn and W. Ho (to be published).
[185] J.R. Hahn and W. Ho, Phys. Rev. Lett. **87**, 196102 (2001).
[186] H.J. Lee and W. Ho, Science **286**, 1719 (1999).
[187] H.J. Lee and W. Ho, Phys. Rev. B **61**, R16347 (2000).
[188] N. Nilius, T.M. Wallis, and W. Ho, J. Chem. Phys. **117**, 10947 (2002), this issue.
[189] H.J. Lee and W. Ho (unpublished results).
[190] J.R. Hahn and W. Ho, Phys. Rev. Lett. **87**, 166102 (2001).
[191] L.J. Lauhon and W. Ho, Faraday Discuss. **117**, 249 (2000).
[192] L.J. Lauhon and W. Ho, J. Phys. Chem. **105**, 3987 (2000).
[193] S.-W. Hla, L. Bartels, G. Meyer, and K.-H. Rieder, Phys. Rev. Lett. **85**, 2777 (2000).
[194] N. Nilius, T.M. Wallis, and W. Ho, Science **297**, 1853 (2002).
[195] O. Pietzsch, A. Kubetzka, M. Bode, and R. Wiesendanger, Science **292**, 2053 (2001).